Jonathan S. Velasco

Finite Element Modeling of Eddy Currents in Uninsulated Laminated-Steel Stacks

School of Electrical Engineering

Thesis submitted for examination for the degree of Master of Science in Technology.

Espoo 04.29.2013

Thesis supervisor:

Prof. Antero Arkkio

Thesis advisors:

Prof. Anouar Belahcen

D.Sc. Paavo Rasilo

Aalto University
School of Electrical
Engineering

AALTO UNIVERSITY
SCHOOL OF ELECTRICAL ENGINEERING

ABSTRACT OF THE
MASTER'S THESIS

Author: Jonathan S. Velasco

Title: Finite Element Modeling of Eddy Currents in Uninsulated Laminated-Steel Stacks

Date: 04.29.2013 Language: English Number of pages:7+76

Department of Electrical Engineering

Professorship: Electromechanics Code: S-17

Supervisor: Prof. Antero Arkkio

Advisors: Prof. Anouar Belahcen, D.Sc. Paavo Rasilo

This thesis deals with the modeling of eddy currents in uninsulated laminations. A numerical model for the calculation of eddy current losses was implemented using finite element analysis. This model calculates the solution from the electric vector potential also known as the T-Ω formulation for the study of eddy current problems. The numerical model was verified by comparing the harmonic solution to different analytical models. Moreover, the results were obtained for non-linear material, i.e. electrical steel.

During the manufacturing process the laminations are stacked and the uneven contact between laminations makes it impossible to assume uniformity in conductivity between adjacent laminations. Electrical conductivity degradation and surface roughness in laminated-steel increases the average iron losses. Whenever the values of inter-laminar conductivity tend to zero, the eddy current component in the direction perpendicular to the lamination vanishes. For this reason, the eddy currents will loop only within the thickness of the lamination and the losses will decrease dramatically for a certain frequency range.

Assuming a linear permeability (low and high) in the inter-laminar region, and widths between 6 μm and 10μm, causes negligible changes in the calculation of the losses for which is recommended to use wider inter-laminar areas and high permeability, as it enhances the convergence of the model.

A model dealing with insulated laminated-stacks was implemented for comparison purposes. Uninsulated laminations could be used as an economical alternative for certain applications where laminated cores are used, as in the case of rotational electrical machines and transformers.

Keywords: Computational Electromagnetics, Finite Element Analysis, Electrical Machines, Iron Losses, Eddy Currents, Steel Laminations

Preface

This research work was conducted at Aalto University School of Electrical Engineering, at the Department of Electrical Engineering, under the supervision of the Electromechanics research group. First of all, I would like to thank my mother, father and sister for their constant support and guidance throughout my personal and professional development, and for showing me the importance of hard work and ethics in life. I am also eternally indebted to Mrs. Lucia Hoffle de Guedez for believing in me and her overall support.They are certainly the most important people in my life and without them I would have never made it.

I am extremely grateful towards all the people involved throughout the development of this thesis work. I would like to thank Prof. Antero Arkkio for having given me the opportunity to join the Electromechanics research group, first through a special assignment, and later on to write my thesis. Prof. Anouar Belahcen and Dr. Paavo Rasilo, were fundamental in the development of my thesis and I would like to express my deepest gratitude to both of them for their patience and time invested in answering my questions. The diligence and kindness of Mr. Ari Haavisto should also be acknowledged.

Last but certainly not least, I would like to thank everyone in the Electromechanics research group for having made this experience to pleasant, in particular my peers Daniel Iruikwu and Sahas Bikram Shah.

Otaniemi, 04.29.2012

Jonathan S. Velasco

Contents

Symbols and abbreviations

Symbols

Vector and matrix quantities are represented in bold, italic, scalar quantities are in italic, and complex-valued quantities, underlined, italic.

A	Magnetic Vector Potential Wb/m, Cross-Sectional Area m^2
a	Magnetic Vector Potential in Linear Combination Wb/m
B	Magnetic Flux Density T
D	Electric Flux Density C/m^2, Dynamic Matrix
E	Electric Field Strength V/m
f	Frequency, General Function
H	Magnetic Field Strength A/m
h	height m
J	Electric Current Density A/m^2
l	Length, Path m
M	Magnetization A/m
N	Shape Function, Number of Turns
P	Jacobian Matrix, Power Loss W/kg
R	Outer Radius m, Resistance Ω
r	Residual
S	Stiffness Matrix
T	Temperature K
t	Time s
u	Electric Vector Potential in Linear Combination A/m
w	Weighting Function
x,y and z	Cartesian Spatial Coordinates m
α	Temperature Coefficient K^{-1}
δ	Depth of Penetration m
θ	Angle Deg
μ	Magnetic Permeability H/m
μ_0	Magnetic Permeability of Vacuum H/m
ν	Reluctivity m/H
ρ	Resistivity Ωm
σ	Electric Conductivity S/m
Φ	Magnetic Flux Wb
ϕ	Electric Scalar Potential Wb/m
Ω	Magnetic Scalar Potential A/m, 2-D Solution Region
ω	Angular Frequency rad/s

Subscripts

Cu	Copper
Fe	Iron
i and j	Nodal Index
lin	Linear
m	Maximum Number of Nodes, Magnetic, Mean
n	Time Step Index
non	Non-linear
p	Peak Value
s	Surface
T	Temperature Dependent
T_o	Toroid

Superscripts

k	Iteration Index
T	Transposed

Abbreviations

2-D	Two-Dimensional
AWG	American Wire Gauge
rms	Root-Mean-Square
SM	Synchronous Machines

1 Introduction

Owing to the nature of the direct-current (DC) excitation of synchronous machines, we may assume that the fundamental flux will not induce currents into the rotor. However, due to the nonlinear nature of commonly-used soft ferromagnetic materials, the permeance harmonic variation, non-sinusoidal mmf and frequency converter supplies, the airgap flux will be distorted and ultimately produce harmonics. These harmonics will induce eddy currents in the laminations, therefore, increasing energy losses which increases temperature of the machine and decreases its overall performance.

Energy dissipation in ferromagnetic materials, frequently referred as iron losses, has been a topic that has drawn researchers attention, for centuries. Analytical formulations have been developed for the separation of the aforementioned losses. Iron losses may be considered as the summation of three independent phenomena: hysteresis, classical eddy currents and excess effects (Bertotti, 1988). These independent effects may also be subdivided into macroscopic and microscopic scale effects. Hysteresis belongs to the microscopic scale effect causing discontinuities in the magnetization. Excess effects are also considered a microscopic scale effect whose impact depends on the material structure and wall domain movement. Lastly, the eddy currents are a macroscopic effect which appears as circulating currents when conducting media is exposed to time-variant magnetic fields.

The lack of devices that can measure each independent overall-loss component makes difficult the verification of this model, in combination with the commonly neglected fact that the accuracy of this model relies on the basic assumption that the flux density is uniformly distributed throughout the material. Therefore, iron loss separation should only be utilized as an approximate conditional expression (Zirka et al., 2010).

Although, iron loss separation has evolved and more elaborate analytical formulations have arised, the relative error between expected and experimental results remains quite large. For this reason many researchers prefer numerical approximations using iterative methods to include the losses in the field solution. Computational electromagnetics has become quite popular nowadays, due to new technological developments which allow heavy computations to be solved faster and in a reliable manner.

Manufacturing costs in the development of electrical machines is rather high, for which laminated cores are commonly used. Rotors in synchronous machines tend to be laminated axially, stacking 1 mm- or 2 mm-thick laminations, to ensure minimal losses. The steady state spatial flux wave rotating at synchronous speeds with the rotor, iron losses within the rotor should ideally be negligible and in many cases considered zero. Unfortunately, rotor eddy currents are caused by harmonics as a reflection of spatial stator winding and slot harmonics, and temporal stator current

harmonics (Hofmann and Sander, 1998).

1.1 Aim of the Work

The main purpose of this work is to study the effect of magnetic hardening due to manufacturing of electrical steel and subsequent variation of inter-laminar electrical conductivity, on eddy-current losses. The model was implemented using 2-D FEM formulations using the cross section of a toroidal magnetic circuit as the study-case geometry.

1.2 Thesis Outline

The outline of this report is as follows:

- Section 1 provides a brief introduction about generalities regarding manufacturing of electrical-steel, energy efficiency and impact in society
- Section 2 reviews relevant literature to the topic. The topics are selected and displayed to ensure understanding and applicability of the work done, starting from the background of electrical-steel manufacturing, eddy-current modeling, selecting the appropriate formulation for our work, insulating coatings and modeling of thin layers and finally the description of inter-laminar effects
- Section 3 introduces the formulation used throughout this work, i.e. electric vector potential. As in the literature most eddy-current formulations rely on the magnetic vector potential, this section derives both equations to display their similarity and ensure mathematical simplicity in our calculations
- Section 4 shows the implementation of the formulation derived in section 3 in computer form using FEM and CAE softwares. Furthermore, the generation of a suitable mesh was sought
- Section 5 presents the design of the magnetic circuit used for the validation of the model as a future work
- Section 6 verifies that the implemented numerical model and the analytical model provide same results in the linear case and that the calculations are performed as accurately as possible
- Section 7 presents the results from the study
- Section 8 conclusion of thesis work

2 Literature Review

This chapter comprises a review of the most relevant articles related to eddy-current losses in laminations and computational electromagnetics, for the completion of this work.

2.1 Electrical Steel

Electrical steel is used in an extensive variety of forms, shapes and properties for the manufacture and implementation of rotational machines and transformers. Although, electrical steel is commonly called iron, it is in fact an alloy processed to magnify the magnetic field acting upon it (Beckley, 2002). Essentially, the magnetization of a material is the response (denoted by the flux density), inherent of a specific specimen to a certain stimulus, i.e. magnetizing field.

The manufacturing of laminated cores is rather critical. Steel sheets are manufactured using rigorous methods to enhance the magnetization and optimize accordingly to the desired application. Iron as a raw material, contains substantial amounts of impurities, some of them need to be extracted or its quantity is decreased, while on the other hand some of them might be beneficial to keep or impractical to remove. For instance, carbon is usually removed during the steel-making process. On the other hand phosphorous in the correct concentrations could affect the final hardness of the steel and the concentration is balanced rather than eliminated. Furthermore, small amounts of silicon contribute to the removal of oxygen which improves the magnetization of the steel, hence decreases the losses. Unfortunately, the overuse of silicon decreases the ductility of the material which makes steel difficult to punch, roll and stack.

Laminations are usually produced using cold- or hot-rolling techniques. The most common method is the cold-rolling as the surfaces are more uniform and the ideal lamination thickness is accomplished easier than in the hot-rolling case. Cold-rolling methods involve the use of cold-rolling mills, hence its name. The steel is fed to the mills through a hot band and rolled until the desired thickness is met. The roll pairs in direct contact with the steel need to be of small radius, as the sought thickness is rather small. Unfortunately, small-radius rolls bend easier than heavy ones, mostly in the middle section of the rolls. To prevent the rolls from producing edge drops, or at least to minimize them, back-up rolls are used (Figure 1). Edge drop is a common occurrence during the cold-rolling process where the areas on the edges of the lamination are thinner than the average thickness of the lamination, usually within 100 mm from the edge (Figure 2). The importance of the lamination thickness needs to be remarked as designers of rotational electrical machines or transformers rely on the number of laminations that will be needed. Hofmann and Sander (1998) explained that the thickness of the sheets can optimize the $\frac{L_d}{L_q}$ ratio of the machine and their capabilities to withstand tremendous centrifugal forces .

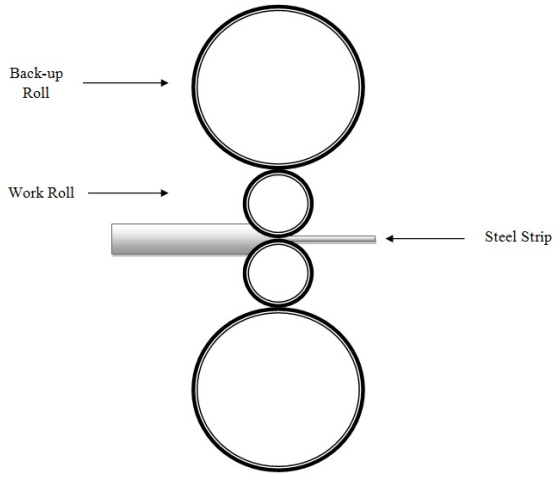

Figure 1: Rolling Mill Representation

Figure 2: Edge Drop Representation

Once the laminations are manufactured, they need to be punched and stacked. The stacking process is also known as core assembly. Laminated cores are fixed prior winding in the case of transformers and in the case of rotational electrical machines, both, winding and mount. The fixing methods vary according to application. The possible fixing techniques are

- Cleating
- Bolting
- Riveting
- Gluing
- Interlocking
- Laser welding in the stamping press
- Electric bead welding
- Die casting of rotors

The description of each individual fixing technique is off topic and wont be described any further. In the case of uninsulated lamination stacks, laser welding and electric bead welding are the most common techniques. For this reason, surface roughness is advised as the stack annealing processes tend to weld laminations together which is highly undesired. Fusing laminations together would increase losses by adding unwanted and random conducting paths. For this reason the working rolls are textured.

Evidently, the manufacturing process degenerates the magnetic properties of the material and needs to be taken into account prior to the implementation of electrical machines, during the design stage. The creation of alloys to improve magnetization does not imply that the desired characteristics will remain unchanged after rolling, punching and stacking. The stress applied on the steel produces inner residual stresses and crystal structure dislocation. Although, the annealing process releases most of the internal stresses, the magnetic hardening inwards the thickness of the lamination is inevitable.

2.2 Modeling of Eddy-current Losses in Electrical Steel Laminations

This subsection will be divided in three parts. Firstly, a brief explanation of iron-loss will be presented, introduction to vector potential formulation in eddy-current problems, and finally the 1-D eddy-current model will be explained.

Iron-Loss Separation

The estimation of core-losses has been a field of study that has intrigued researchers for decades as the modeling of these, tend quite complex. Furthermore, core-losses estimation models have been presented in the literature multiple times, seeking for a standard and efficient method to predict losses to enhance machine-design techniques.

Formerly, the average power loss per unit volume P_{core} of any material was commonly calculated as the contribution of hysteresis and a so-called dynamic contribution. The idea behind the loss separation is the segregation of contributions based on the physical standpoint, i.e., macroscopic, microscopic. The hysteresis contribution originates at a microscopic level, whereas the dynamic contribution was considered as a macroscopic phenomena. Under sinusoidal flux and assuming homogeneous magnetization in space, the dynamic-loss contribution may be interpreted as the nowadays called classical-losses which disregards any domain wall motion and skin effect. Owing to the difference between estimated classical losses and the measured ones, being the later ones greater, it was noticed that the model was over-simplified and that the domain walls motion needed to be quantified. Hence, the introduction of excess losses into the model, formerly known as anomalous losses.

Bertotti (1988), proposed a statistical loss-separation model that has been widely accepted by many authors. This statistical model attributes the difference between the measured losses and the estimated losses to the presence of excess losses. The model decomposed core-losses as a sum of independent loss contributions, i.e., hysteresis, classical eddy-current, and excess losses.

$$P_{\text{core}} = P_{\text{hys}} + P_{\text{class}} + P_{\text{exc}} \tag{2.1}$$

where the sum of the classical eddy-current and excess losses is interpreted as the macroscopic and microscopic phenomena encountered during the magnetization process, respectively. Moreover, these quantities obey power functions of the flux density $\hat{B}$ and the magnetizing frequency f under the assumption of sinusoidal flux

$$P_{\text{core}} = c_{\text{hys}} f \hat{B}^2 + c_{\text{class}} f^2 \hat{B}^2 + c_{\text{exc}} f^{3/2} \hat{B}^{3/2} \tag{2.2}$$

The classical loss coefficient is calculated from an analytical expression in terms of the electrical conductivity σ and the thickness of the lamination d

$$c_{\text{class}} = \frac{\sigma d^2 \pi^2}{6} \tag{2.3}$$

whereas the hysteresis and excess loss coefficients are determined through experimental data. Unfortunately, this model seems to function only under the previously mentioned assumption of uniform magnetization under sinusoidal flux and it seems to be consistent only in the linear case, however, the flux density distribution might not be homogeneous and it hardly ever varies sinusoidally with time (Overshott et al., 1968; Zirka et al., 2010). Mayergoyz et al. (1984) mentioned that for linear media the type of polarization of the incident wave, i.e., magnetic flux, does not play a major role and the incident wave can be expressed as a linear combination.

The relative error between the loss-separation model and the results obtained by measurements is undoubtedly high and cannot be neglected. Many authors have stated that the main reason can be attributed partially due to the uniformity assumption however, if a non-uniformity model, including skin effect is implemented, with accurate modeling of eddy currents within laminations, satisfying results are obtained. In the literature some authors state that the inclusion of the skin effect in the field problem can be obtained by the appropriate modeling of the flux density distribution, which partially explains the presence of the so-called excess eddy-current losses (Mayergoyz and Serpico, 1999).

Vector Potential Formulation in Eddy-Current Problems

Evidently, in more complex geometries, the assumption of infinite laminations is not applicable and a more comprehensive expression needs to be formulated. The vector potential formulation is the most common approach to more complex geometries and comprehensive case scenarios involving 3-D-time-dependent problems. Furthermore, the use of the vector potential formulation in the study of 2-D field problems simplifies calculations, as the field component reduces to a single-component variable (Luomi, 1993). This mathematical approach is commonly used for solving the field problem and formulating eddy current models by coupling them to Maxwell's equations, generally in quasi-static form. Traditionally, two formulations for the modeling of eddy currents are found in the literature: the magnetic vector potential and the electric vector potential formulations.

The magnetic vector potential formulation, commonly known as $A - \phi$ formulation couples the magnetic flux density and the magnetic vector potential. Moreover,

the current density is usually unknown and another relationship needs to be found. For this reason, the electric field is implicitly derived in terms of the magnetic vector potential A and a reduced electric scalar potentialϕ. The electric scalar potential is directly associated with the induced voltage, hence, the magnetic vector potential is usually associated with voltage-source driven circuits. The use of the magnetic vector potential will not be presented in the literature review as the focus of this work is on the application and advantages of the use of the electric vector potential in the modeling of eddy currents. However, the magnetic vector potential formulation will be presented in the methods.

The $T-\Omega$ formulation is based on the electric vector potential which is coupled to the reduced magnetic scalar potential in the conducting region and on the reduced magnetic scalar potential alone in the non-conducting region as the induced field is irrotational (Keskinen, 1990). The vector potential is specified so that the Coulomb gauge is zero

$$\nabla \cdot \boldsymbol{T} = 0 \tag{2.4}$$

This ensures the uniqueness of the vector field and allows the calculation of the induced currents in the domain. Furthermore, the Lorentz gauge can also be applied for uniqueness purposes

$$\nabla \cdot \boldsymbol{T} = \sigma\mu\frac{\partial\Omega}{\partial t} \tag{2.5}$$

Equation 2.5 however, works under the assumption of homogeneous electrical conductivity and permeability in the conducting regions. By using Lorentz gauge it is possible to decouple the electric vector potential and the magnetic scalar potential. In this work however, Coulomb gauge will be implemented in the formulation as the model is based on a non-conducting region. Furthermore, due to the importance of the T-Ω formulation throughout this work, its advantages will be presented in its own section

1-D Eddy-Current Model

The thickness and high conductivity of steel sheets represent a major factor in the presence of the skin effect and it needs to be taken into account, thus simplified models assuming uniform flux density distribution in the lamination cross-section cannot be implemented, if accurate results are sought. Moreover, the induced eddy currents seem to be extremely high whenever the machine is driven by a frequency converter, and due to the relationship between the magnetizing frequency and the skin effect, an accurate study of these cases needs to be considered. Dlala and Arkkio (2008) and Pippuri (2010) implemented a 2-D$-$1-D coupled method where the skin effect is modeled in the 1-D finite element model and it is coupled to the 2-D model via a fixed-point procedure, i.e., nested iteration. This case not only provides an accurate estimation of the flux density distribution but also simplifies

what otherwise would had been modeled with a three-dimensional approach, using Maxwell equations. Assuming no return path of eddy currents due to the assumption of infinite length of the lamination, the field problem can be reduced to the diffusion equation (Vecchio, 1982; Mayergoyz et al., 1984)

$$\frac{\partial^2 \boldsymbol{h}(z,t)}{\partial z^2} = \sigma \frac{\partial \boldsymbol{b}(z,t)}{\partial t} \tag{2.6}$$

where $\boldsymbol{h}$ and $\boldsymbol{b}$ are the magnetic field strength vector and the magnetic flux density vector, which are coupled through their material characteristics, i.e., $\boldsymbol{b}$-$\boldsymbol{h}$ loop, σ is the electric conductivity of the material, z the cartesian coordinate in the direction of the thickness of the lamination, and lastly t stands for time.

2.3 T-Ω Formulation for Eddy Current Modeling

The use of the electric vector potential in the study of thin laminations and lamination stacks has been presented multiple times in the literature Menana and Feliachi (2011),Nakata et al. (1988) and Codecasa et al. (2010). Nakata et al. (1988) explained the benefit of using the electric vector potential in the modeling of 3-D eddy currents. Furthermore, this mathematical approach is especially effective in non-conducting regions and since the magnetic fields produced by the magnetizing currents and eddy currents are calculated by the electric vector potential coupled to a magnetic scalar potential, the implementation of two extra scalar potentials is unnecessary and the calculation is simplified. This formulation can be used for both, eddy currents and magnetizing currents decreasing computational cost as the integration of the source field from Biot-Savart's law is not required. Ren (2002) and Kotiuga (1987) studied the case of conductors with holes, such as in multiply connected domains, the use of the electric vector potential can be quite challenging as convergence problems may arise whenever conductivities tend to zero. This is evident as whenever sigma tends to zero, $\frac{1}{\sigma}$ tends to infinity .

Nakata et al. (1988) mentioned that the common use of the magnetic vector potential in 2-D cases is traditionally extended to 3-D geometries, which increases the number of unknowns, hence, computational time. If the conducting and non-conducting regions are studied separately, the implementation of the electric vector potential formulation could improve considerably computational time and enhance convergence of the solution. Furthermore, if the magnetizing currents flow two-dimensionally, i.e. x- and y-direction, the x- and y- components of the electric vector potential become zero and the vector potential can be considered as a single-value term in the z-direction.

In recent literature T-Ω formulation has also been found to be a useful tool in modeling of eddy currents in multiply connected regions (Ren, 2002). The use of the

scalar potential is advantageous as the number of unknowns are reduced, however in a multiply connected regions, this assumption is not correct as it is found that the scalar potential is multivalued. For this reason, Ampere's law must be ensured and this can be done by implementing the so-called cuts connecting conducting and non-conducting regions through a low conductivity element to allow a coupling scalar potential. The main concern regarding Ampere's law is that the line integral of the domain cannot be considered as zero as one domain is contained in another which, would mean the use of two different integrals independently for each region, conduction and non-conducting. To preserve zero curl condition it is necessary to ensure one degree of freedom per cutting domain only at the edges connecting both domains.

The use of electric vector potential in multiply connected regions is disadvantageous as it requires the implementation of cutting domains or filling techniques, where holes are modeled as conductors with low conductivity, increasing the number of unknowns. In the case of laminated structures, such as transformers and laminated cores, where the currents are assumed to be 2-dimensional, the case of one-component electric vector potential formulation is rather encouraged as the accuracy tends to be high while preserving 2-dimensional current flow, hence the net current adds up to zero and reduces the number of unknowns.

2.4 Insulating Coatings, Electrical Conductivity and Interlaminar Effects

Eddy currents are traditionally reduced in electrical machines and transformers by laminating their magnetic core. Moreover, it is common to increase the resistivity between adjacent laminations by adding insulating coatings. This splits the induced currents into separate paths which ultimately reduces the eddy current losses, improving machine performance. The type of insulation needs to be evaluated as it varies depending on the application and thickness of the laminations to stack. The properties of coatings can be divided into two: primary and secondary properties. Coombs et al. (2001) consider that the primary attributes are those related to the enhancement of the characteristics of the electrical steel substrate and the secondary are the specific application which is needed for. To have a better understanding has classified the primary and secondary properties as followed

Primary Properties

- Insulation Resistance
- Punchability
- Corrosion Resistance

Secondary Properties

- Weldability
- Heat Resistance
- Stacking Factor
- Resistance to Chemicals
- Burn-out to Chemicals
- Resistance to Compression
- Scratch Resistance / Scuff Resistance
- Adhesion - Resistance to Tension or Bending Stress

A documented comparison of losses measured in a small motor using coated and uncoated steels is presented by Coombs et al. (2001), showing not much of a difference between having uncoated steels or thin coating as long as there is no presence of burrs. Furthermore, the electromotive inter-laminar forces need to reach a certain threshold to have a representative impact on the losses. In bigger machines this would not be an issue as coating is generally thicker to prevent inter-laminar short circuits. Unfortunately, thick coatings have a considerable impact on the stacking factor of the machine, hence, on the dimensions of the stator and/or rotor. Furthermore, the increment in the thickness of the insulation decreases the ideal stacking which increases the excitation currents.

Determining the conductivity and relative permeability of thin laminated-materials is quite a challenging task, these usually being obtained through experimental data measuring lamination stacks. The most common way to find the permeability of the material is by measuring the flux and constructing the B-H loop, also known as magnetization curve, of the specimen (Tosaka et al., 2005; Yating et al., 2011). Tosaka et al. (2005) presented a method to determine the relative permeability and conductivity of a specimen based in the shielding effectiveness of the material. This study confirmed that the variance of the conductivity at different frequencies is negligible, hence, the conductivity of the material should be considered a global quantity. It was also found that the nominal values of the relative permeability in ferromagnetic materials are just as accurate as the ones calculated from the B-H curve. Moreover, in a frequency range between 500 Hz and 20 kHz the nominal value of the relative permeability does not seem to vary.

Bjerkan (2005) states that at low frequencies the induced electrical field between laminations is low and for that reason the resistive current is also low. Evidently, the impact of the type of insulation and its thickness will have an impact on the induced-current path. Moreover, at higher frequencies the effect will be opposite and as the inter-laminar currents become stronger, a greater loop is formed at the edges of the stack. Since the currents in the inter-laminar region move only

perpendicularly to the lamination, a 2-D approximation is possible by coupling the field problem in 2-D with a 1-D finite element model as previously mentioned.

The conductivity of the insulation can be calculated analytically if the surface resistance is known. The analytical expression to calculate the inter-laminar conductivity is

$$\sigma = \frac{(1 - \zeta_{Fe})d}{\rho} \tag{2.7}$$

where $\zeta_F e$ is the lamination stacking factor, d is the thickness of the lamination and ρ is the resistance in Ωm^2. From this analytical expression is inevitable to realize that increasing the thickness will also increase the inter-laminar conductivity, hence, the appropriate coating needs to be selected depending on the thickness of the lamination, induced voltage and application.

3 Numerical Methods

Geometries in electrical machines are generally complex and the magnetization occurs as a time-dependent, three-dimensional phenomenon, which makes the solution of the magnetic field in electrical machines undoubtedly challenging. Furthermore, magnetic properties of the material must be taken into account as non-linearities appear due to permeance harmonic variation and non-sinusoidal mmf. Hence, the equations are also non-linear and must be coupled with constitutive relations to maintain the accuracy of the model.

The limiting capabilities of analytical techniques have impulsed the developing of iterative methods for solving differential equations for the modeling of eddy currents, including the losses using a magneto dynamic model. These electromagnetic models rely on solving the Maxwell differential equations.

3.1 Two-dimensional Eddy Current Model of Steel Laminations

The solution of the field problem is shown for both, time-stepping and time-harmonic cases. The 2-D eddy current formulation is obtained from the quasi-static Maxwell's equations.

Owing to the nature of the Euclidean geometry used in this work, first-order triangular elements for potential problems have been sufficient for the case study. Moreover, although the eddy currents were computed using the electric vector approach, both cases will be derived and compared.

3.2 Maxwell Equations and Constitutive Relations

Maxwell Equations

Maxwell equations are presented in differential form. Although, they are commonly known, they will be displayed below to provide easier references to equations for the development of the 2-D eddy-current model below.

Faraday's Law of Induction

$$\nabla \times \boldsymbol{E} = -\frac{\partial \boldsymbol{B}}{\partial t} \tag{3.1}$$

Ampere's Law

$$\nabla \times \boldsymbol{H} = \boldsymbol{J} + \frac{\partial \boldsymbol{D}}{\partial t} \tag{3.2}$$

Gauss' Law for Electricity

$$\nabla \cdot \boldsymbol{D} = \rho \tag{3.3}$$

Gauss' Law for Magnetism

$$\nabla \cdot \boldsymbol{B} = 0 \tag{3.4}$$

Constitutive Relations

The constitutive relations are presented to show the relationship of Maxwell equations with the characteristics of the material

$$\boldsymbol{J} = \sigma \boldsymbol{E} \tag{3.5}$$

$$\boldsymbol{B} = \mu \boldsymbol{H} \tag{3.6}$$

$$\boldsymbol{D} = \epsilon \boldsymbol{E} \tag{3.7}$$

3.3 Magnetic Vector Potential Formulation

The magnetic vector potential is a vector field with no time-varying charge distribution, defined by 3.8. This approach is commonly used in the literature for modeling eddy currents as it ensures Gauss's law since the divergence of the curl equals zero (3.4). The magnetic vector potential formulation is expressed as

$$\boldsymbol{B} = \nabla \times \boldsymbol{A} \tag{3.8}$$

where $\boldsymbol{B}$ is the magnetic flux density and $\boldsymbol{A}$ is the magnetic vector potential.

where $\boldsymbol{H}$ is the magnetic field strength and μ is the permeability of the material, which in the case of ferromagnetic materials is not a constant but rather a function of the magnetic field strength. Equation (3.9) can also be written as

$$\boldsymbol{H} = \nu \boldsymbol{B} \tag{3.9}$$

in this case ν being the reluctivity of the material and a function of magnetic flux density.

Substituting equation (3.8) into equation (3.9) we obtain an expression of the magnetic field strength in terms of the reluctivity of the material and the magnetic vector potential.

$$\boldsymbol{H} = \nu \nabla \times \boldsymbol{A} \tag{3.10}$$

This expression allows us apply Amperes' law for the calculation of the current density, i.e., induced eddy currents. Considering a quasi-static problem, the electric displacement is neglected and the eddy-current problem can be presented in terms of the magnetic vector potential

$$\boldsymbol{J} = \nabla \times (\nu \nabla \times \boldsymbol{A}) \tag{3.11}$$

Since the eddy currents are unknown, another relationship needs to be build in order to solve the differential equation. The magnetic vector potential also ensures Faraday's law and equation (3.1) can be expressed as

$$\nabla \times \boldsymbol{E} = -\nabla \times \frac{\partial \boldsymbol{A}}{\partial t} \tag{3.12}$$

where $\boldsymbol{E}$ is the electric field strength. The electric field strength can be solved by using a electric scalar potential

$$\boldsymbol{E} = -\frac{\partial \boldsymbol{A}}{\partial t} - \nabla\phi \tag{3.13}$$

Substituting equation (3.13) into constitutive equation (3.5)

$$\boldsymbol{J} = -\sigma\frac{\partial \boldsymbol{A}}{\partial t} - \sigma\nabla\phi \tag{3.14}$$

and finally, we may set equations (3.11) and (3.14) as equal giving us the general 3-D form of the eddy-current A-ϕ formulation.

$$\nabla \times (\nu\nabla \times \boldsymbol{A}) = -\sigma\frac{\partial \boldsymbol{A}}{\partial t} - \sigma\nabla\phi \tag{3.15}$$

For simplicity and visual purposes equation (3.15) will be derived, solving the curl of the curl into a second order derivative. By doing this the direction and cartesian-components are shown and ensured for our specific model, i.e., 1-D Eddy-current model. Since, the general form is presented as a 3-D eddy-current model, all directions and cartesian coordinates x,y,z will be shown during the derivation

$\hat{i}$-direction

$$\frac{\partial}{\partial y}(\nu\frac{\partial A_y}{\partial x}) - \frac{\partial}{\partial y}(\nu\frac{\partial A_x}{\partial y}) + \frac{\partial}{\partial z}(\nu\frac{\partial A_z}{\partial x}) - \frac{\partial}{\partial z}(\nu\frac{\partial A_x}{\partial z}) = -\sigma\frac{\partial A_x}{\partial t} \tag{3.16}$$

$\hat{j}$-direction

$$-\frac{\partial}{\partial x}(\nu\frac{\partial A_y}{\partial x}) + \frac{\partial}{\partial x}(\nu\frac{\partial A_x}{\partial y}) - \frac{\partial}{\partial z}(\nu\frac{\partial A_y}{\partial z}) + \frac{\partial}{\partial z}(\nu\frac{\partial A_z}{\partial y}) = -\sigma\frac{\partial A_y}{\partial t} \tag{3.17}$$

$\hat{k}$-direction

$$-\frac{\partial}{\partial x}(\nu\frac{\partial A_z}{\partial x}) + \frac{\partial}{\partial x}(\nu\frac{\partial A_x}{\partial z}) - \frac{\partial}{\partial y}(\nu\frac{\partial A_y}{\partial z}) + \frac{\partial}{\partial y}(\nu\frac{\partial A_z}{\partial y}) = -\sigma\frac{\partial A_z}{\partial t} \tag{3.18}$$

As mentioned before, the field formulation is studied within the thickness of the lamination. After simplifying our equations we obtain

$\hat{i}$-direction

$$\frac{\partial}{\partial z}(\nu\frac{\partial A_x}{\partial z}) = -\sigma\frac{\partial A_x}{\partial t} \tag{3.19}$$

$\hat{j}$-direction

$$\frac{\partial}{\partial z}(\nu\frac{\partial A_y}{\partial z}) = -\sigma\frac{\partial A_y}{\partial t} \tag{3.20}$$

3.4 Electric Vector Potential Formulation

Firstly, the divergence of the current density must be ensured.

$$\nabla \cdot \boldsymbol{J} \ = 0 \tag{3.21}$$

In this fashion it is evidently that the curl of the vector potential will describe the behavior of the induced currents within the material as it satisfies the condition defined by equation (3.21).

$$\boldsymbol{J} = \nabla \times \boldsymbol{T} \tag{3.22}$$

Substituting equation (3.2) in equation (3.22) we obtain that the curl of the field strength is the same as the curl of the electric vector potential

$$\nabla \times \boldsymbol{H} = \nabla \times \boldsymbol{T} \tag{3.23}$$

In the presence of no source in the domain of study, the magnetic field and the electric vector potential are coupled with the magnetic scalar potential

$$\boldsymbol{H} = \boldsymbol{T} - \nabla\Omega \tag{3.24}$$

As the number of unknowns in a system of equations needs to be equal or less than the number of equations, it is necessary to formulate another relationship that can allow the solution to be computed. The constitutive equation (3.5) relates the current density in the material and the electric field.

$$\boldsymbol{E} = \frac{\nabla \times \boldsymbol{T}}{\sigma} \tag{3.25}$$

By taking the curl of the electric field we obtain a full expression that models the eddy currents in a closed region.

$$\nabla \times \frac{\nabla \times \boldsymbol{T}}{\sigma} = \frac{\partial \mu \boldsymbol{T} - \nabla\Omega}{\partial t} \tag{3.26}$$

For the specific purposes of this thesis work, the expression has been expanded to provide with the specific formulation needed to ensure the induction of a magnetic field in the z-direction.

$$\begin{aligned}\nabla \times \frac{\nabla \times \boldsymbol{T}}{\sigma} = \frac{1}{\sigma}[&(\frac{\partial^2 T_y}{\partial x \partial y} - \frac{\partial^2 T_x}{\partial z^2} - \frac{\partial^2 T_x}{\partial y^2} + \frac{\partial^2 T_z}{\partial x \partial z})\hat{i} \\ &+(-\frac{\partial^2 T_y}{\partial x^2} - \frac{\partial^2 T_y}{\partial z^2} + \frac{\partial^2 T_x}{\partial x \partial y} + \frac{\partial^2 T_z}{\partial y \partial z})\hat{j} \\ &+(-\frac{\partial^2 T_z}{\partial x^2} - \frac{\partial^2 T_z}{\partial y^2} + \frac{\partial^2 T_x}{\partial y \partial z} + \frac{\partial^2 T_y}{\partial x \partial z})\hat{k}]\end{aligned} \tag{3.27}$$

Finally, the expression below describes the variation of the current density (in x- and y-direction) whenever the electric vector potential is applied in the z-direction.

$\hat{k}$-direction

$$\frac{1}{\sigma}[-\frac{\partial^2 T_z}{\partial x^2} - \frac{\partial^2 T_z}{\partial y^2}] = -\frac{\partial(\mu T_z)}{\partial t} \tag{3.28}$$

As we observe from the derivation of both, magnetic and electric vector potential for the study of eddy-current losses in the x-y plane, the use of the electric vector potential simplifies the formulation by having to solve the vector potential only in one direction, ensures the divergence of the current densities and reducing the number of unknowns. The initial boundary condition can also be imposed uniformly around the edges of the lamination, unlike the case of the magnetic vector potential.

3.5 Time Harmonic Solution

Whenever the domain of study is considered magnetically linear, a sinusoidally varying source, i.e. potential difference or source current, induces a purely sinusoidal field. Hence, the time differentiation may be replaced by $j\omega$ and the physical quantities can be obtained in terms of complex phasors.

Magnetic Vector Potential

$$\frac{\partial \boldsymbol{A}}{\partial t} = j\omega \underline{A} \tag{3.29}$$

Electric Vector Potential

$$\mu \frac{\partial \boldsymbol{T}}{\partial t} = j\omega\mu \underline{T} \tag{3.30}$$

The harmonic solution vector plot of the currents estimated using the electric vector potential and a field strength source of 1200 A/m is displayed below. The model consists of 20 steel-sheets with a thickness of 1 mm and an inter-laminar width of 6 μ. The height and width of the laminated-stack, are the same and is proportional to the amount of sheets used in the studied geometry.

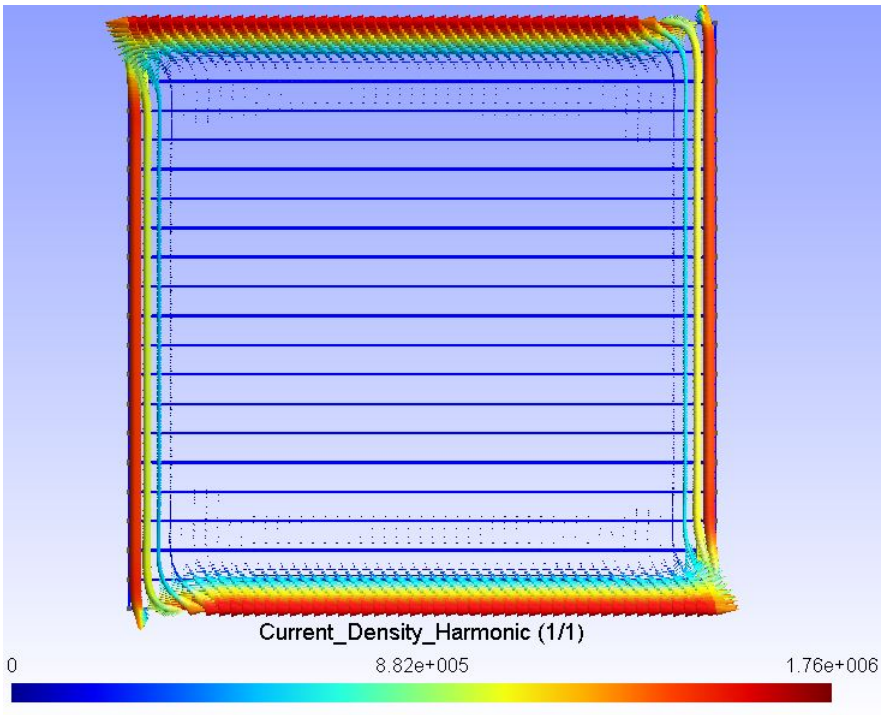

(a) Inter-laminar Conductivity $\sigma = 8.5$ MS/m

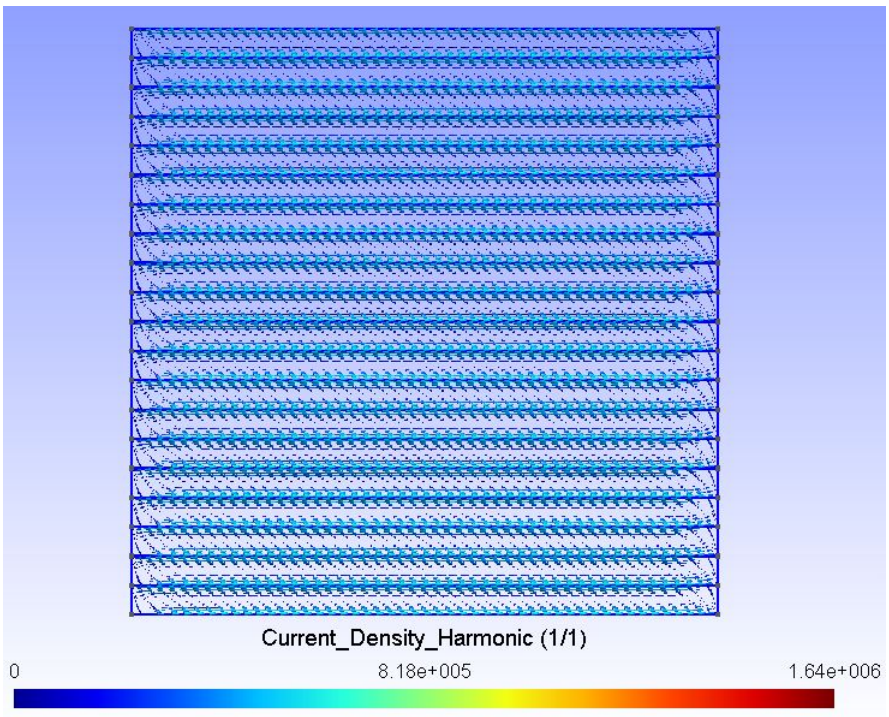

(b) Inter-laminar Conductivity $\sigma \approx 0$ S/m

Figure 3: Current Vector Plot - Harmonic Solution 50 Hz

3.6 Field Problem Discretization

Owing to the complexity of the mathematical representation of the field problem (non-linear), the solution is commonly obtained with the aid of computers. For this reason the above presented equations need to be presented in discretized form in space and time.

3.6.1 Time Discretization

There are multiple methods commonly used to discretize equations with respect to time. The selection of the a specific discretization method, i.e., Crank-Nicholson, Backward Euler, etc., will have a direct influence on speed of convergence, and accuracy of the solution.

Backward euler was selected as the time discretization method for this work, due to its computational speed capabilities. In the previous subsection, it has been shown that the study is being ensured to be within the thickness of the lamination. For this reason the magnetic vector potential will be represented as A instead, in association with a constant time-step of length Δt.

In equation (3.15) we observe that the right side of the equation is constituted by a time dependent factor and a scalar function. In the 2-D problem, the variation of the flux in the -z direction is considered negligible, and the reduced $\nabla\phi$ vanishes. The time discretized expression is

$$\frac{\partial A^k}{\partial t}|_{n+1} = \frac{A^k_{n+1} - A^k_n}{\Delta t} \tag{3.31}$$

where k represents the iteration number index and n is the time step index.

3.6.2 Space Discretization

The space discretization is computed by using Garlekin's method, which is a variation of the method of weighted residuals. To be able to apply Garlekin's method, it is necessary to rewrite the formulation shown in (3.19) and (3.20) in the most suitable form for spatial discretization, i.e., weak form. The differential $\frac{\partial}{\partial z}$ can be expressed as ∇ leading to the weak form representation

$$\nabla \cdot (\nu^k_{n+1} \nabla A^k_{n+1}) - \sigma \frac{A^k_{n+1} - A^k_n}{\Delta t} = 0 \tag{3.32}$$

Applying the weight of residuals method we multiply the whole expression by a weight function and integrate the expression over the domain.

$$\int_\Omega (w(\nabla \cdot \nu^k_{n+1} \nabla A^k_{n+1}) - w\sigma \frac{A^k_{n+1} - A^k_n}{\Delta t}) \mathrm{d}\Omega = 0 \tag{3.33}$$

The distributive property is applied and the expression is expanded

$$\int_{\Omega}(\nabla\cdot(w\nu_{n+1}^{k}\nabla A_{n+1}^{k})-\nu_{n+1}^{k}\nabla w\cdot\nabla A_{n+1}^{k}-w\sigma\frac{A_{n+1}^{k}-A_{n}^{k}}{\Delta t})\mathrm{d}\Omega=0 \tag{3.34}$$

once again, the divergence term vanishes at the boundary

$$\int_{\Omega}(-\nu_{n+1}^{k}\nabla w\cdot\nabla A_{n+1}^{k}-w\sigma\frac{A_{n+1}^{k}-A_{n}^{k}}{\Delta t})\mathrm{d}\Omega=0 \tag{3.35}$$

rewriting the vector potential as a linear combination of the shape functions we obtained

$$A_{n}^{k}=\sum_{i=1}^{m}a_{i,n}^{k}N_{i} \tag{3.36}$$

substituting (3.36) into equation (3.35) and after minor mathematical manipulation, and substitution of the weight function by their shape function, i.e., Garlekin's method, we obtain the weak space-discretized form

$$\sum_{i=1}^{m}\int_{\Omega}(-\nu_{n+1}^{k}\nabla N_{j}\cdot\nabla N_{i}a_{i,n+1}^{k}-N_{j}N_{i}\sigma\frac{a_{i,n+1}^{k}-a_{i,n}^{k}}{\Delta t})\mathrm{d}\Omega=0 \tag{3.37}$$

Finally, the expression can be expressed in matrix form, where $\boldsymbol{S}$ is the stiffness matrix and $\boldsymbol{D}$ the dynamic matrix

$$\boldsymbol{Sa}+\frac{1}{\Delta t}\boldsymbol{Da}=0 \tag{3.38}$$

hence,

$$S_{ji,n+1}^{k}=\int_{\Omega}\nu_{n+1}^{k}(\nabla N_{j}\cdot\nabla N_{i})\mathrm{d}\Omega \tag{3.39}$$

$$D_{ji,n}^{k}=\int_{\Omega}\sigma N_{j}N_{i}\mathrm{d}\Omega=D_{ji,n+1}^{k} \tag{3.40}$$

Electric Vector Potential

Similarly, using the method of weighted residuals in the time-stepped expression of the electric vector potential formulation

$$\nabla\cdot(\frac{1}{\sigma}\nabla T_{n+1}^{k})-\frac{\mu_{n+1}^{k}T_{n+1}^{k}-\mu_{n}^{k}T_{n}^{k}}{\Delta t}=0 \tag{3.41}$$

Decomposing the electric vector potential into the linear combination of the shape functions

$$T_{n}^{k}=\sum_{i=1}^{m}u_{i,n}^{k}N_{i} \tag{3.42}$$

Finally, we substitute (3.42) in (3.41) and we obtain a similar equation to the one presented in (3.37)

$$\sum_{i=1}^{m}\int_{\Omega}(-\frac{1}{\sigma}\nabla N_j\cdot\nabla N_i u_{i,n+1}^k - N_jN_i\frac{\mu_{n+1}^k u_{i,n+1}^k-\mu_n^k u_{i,n}^k}{\Delta t})\mathrm{d}\Omega = 0 \tag{3.43}$$

which can be represented in matrix form where,

$$S_{ji,n+1}^k = \int_{\Omega}\frac{1}{\sigma}(\nabla N_j\cdot\nabla N_i)\mathrm{d}\Omega \tag{3.44}$$

$$D_{ji,n}^k = \int_{\Omega}\mu_n^k N_jN_i\mathrm{d}\Omega \tag{3.45}$$

$$D_{ji,n+1}^k = \int_{\Omega}\mu_{n+1}^k N_jN_i\mathrm{d}\Omega \tag{3.46}$$

3.7 Methods for Solving Nonlinear Systems of Equations

Since our solution involves sources on nonlinearities, i.e., feromagnetic materials, the solution needs to be carried out iteratively by linearization at each iteration. Since, the analysis of eddy currents can be carried out by describing a single-valued magnetization $B(H)$ curve - and as long as the number of equations matches the number of unknowns - The Newton-Raphson solution may be used for this purpose by defining a residual vector and defining the appropriate boundary conditions.

The residual must be forced to be zero, and iterations will be carried until this condition is satisfied. Every iteration is set at a value of $k+1$, a new vector of the nodal values will be constructed by correcting the solution from the previous iteration k

$$\boldsymbol{a}^k = \boldsymbol{a}^{k-1} + \Delta\boldsymbol{a}^k \tag{3.47}$$

where the residual is calculated as

$$\boldsymbol{r}(\boldsymbol{a}^{k-1}+\Delta\boldsymbol{a}^k) = 0 \tag{3.48}$$

it is important to notice that the term $a^{k-1}+\Delta a^k$ is spatial dependent on each node over the domain, i.e., Taylor approximation

$$\begin{aligned} r(a_1^{k-1}+\Delta {a_1}^k \ldots a_m^{k-1}+\Delta a_m^k) \simeq r(a_1^{k-1}\ldots a_m^{k-1})+ \\ \frac{\partial r}{\partial a_1}|_{a_1=a_1^{k-1}}\Delta a_1^k + \ldots \frac{\partial r}{\partial a_m}|_{a_m=a_m^{k-1}}\Delta a_m^k = 0 \end{aligned} \tag{3.49}$$

hence,

$$\boldsymbol{r}(\boldsymbol{a}^{k-1}+\Delta\boldsymbol{a}^k) = \boldsymbol{r}(\boldsymbol{a}^{k-1}) + \frac{\partial\boldsymbol{r}}{\partial\boldsymbol{a}}|_{\boldsymbol{a}=\boldsymbol{a}^{k-1}}\Delta\boldsymbol{a}^k = 0 \tag{3.50}$$

The derivative of the residual with respect to the potential can be expressed as a matrix variable $\boldsymbol{P}$. This term is the so-called Jacobian matrix

$$\boldsymbol{P} = \frac{\partial \mathbf{r}}{\partial \mathbf{a}} \tag{3.51}$$

Substituting (3.51) back into (3.50)

$$\boldsymbol{r}(\boldsymbol{a}^{k-1} + \Delta \boldsymbol{a}^k) = \boldsymbol{r}(\boldsymbol{a}^{k-1}) + \boldsymbol{P}|_{\boldsymbol{a}=\boldsymbol{a}^{k-1}} \Delta \boldsymbol{a}^k = 0 \tag{3.52}$$

The Jacobian matrix tends to be hard to invert, therefore, it is commonly calculated from the residual equation

$$\boldsymbol{P} \Delta \mathbf{a}^k = -\boldsymbol{r}(\mathbf{a}^{k-1}) \tag{3.53}$$

Represented as a matrix,

$$\begin{bmatrix} \boldsymbol{P}_{xx}(\boldsymbol{a}^k) & \boldsymbol{P}_{xy}(\boldsymbol{a}^k) \\ \boldsymbol{P}_{yx}(\boldsymbol{a}^k) & \boldsymbol{P}_{yy}(\boldsymbol{a}^k) \end{bmatrix} \begin{bmatrix} \Delta \boldsymbol{a}_x^k \\ \Delta \boldsymbol{a}_y^k \end{bmatrix} = - \begin{bmatrix} \boldsymbol{r}_x(\boldsymbol{a}_x^k) \\ \boldsymbol{r}_y(\boldsymbol{a}_y^k) \end{bmatrix} \tag{3.54}$$

Magnetic Vector Potential

For visual purposes, the Jacobian matrix will be derived from equation (3.38). First expressing the residual expression

$$\boldsymbol{r}(\boldsymbol{a}) = \boldsymbol{S}\boldsymbol{a} + \frac{1}{\Delta t}\boldsymbol{D} - \boldsymbol{f} = 0 \tag{3.55}$$

By taking the derivative of the residual with respect to the vector potential we obtain the Jacobian matrix

$$\frac{\partial \boldsymbol{r}(\boldsymbol{a})}{\partial \boldsymbol{a}} = \boldsymbol{S} + \frac{\partial \boldsymbol{S}}{\partial \boldsymbol{a}}\boldsymbol{a} + \frac{1}{\Delta t}\boldsymbol{D} + \frac{1}{\Delta t}\frac{\partial \boldsymbol{D}}{\partial \boldsymbol{a}}\boldsymbol{a} \tag{3.56}$$

After simple algebraic manipulation the final expression of the Jacobian matrix in terms of the stiffness matrix and dynamic matrix and time-discretized

$$\frac{\partial \boldsymbol{r}(\boldsymbol{a})}{\partial \boldsymbol{a}} = \boldsymbol{S} + \frac{\partial \boldsymbol{S}}{\partial \boldsymbol{a}}\boldsymbol{a} + \frac{1}{\Delta t}\boldsymbol{D} \tag{3.57}$$

Electric Vector Potential

$$\frac{\partial \boldsymbol{r}(\boldsymbol{u})}{\partial \boldsymbol{u}} = \boldsymbol{S} + \frac{1}{\Delta t}\boldsymbol{D} + \frac{1}{\Delta t}\frac{\partial \boldsymbol{D}}{\partial \boldsymbol{u}}\boldsymbol{u} \tag{3.58}$$

4 Computational Approach

The solution of the field problem requires complex calculations that would be impossible to perform without the use of computers. Analytical solutions lack accuracy as geometries tend to be quite complex, hence approximate solutions using numerical methods and refined meshes seem to be the most suitable choice. Unfortunately, approximate solutions require the implementation of iterative methods where, computer memory plays an important role in the development of efficient algorithms and computational speed.

Generally, the stages undergone in the field problem approximation can be classified into: pre-processing, solution and post-processing. However, in this work, the design of the magnetic circuit has been included for verification of our mathematical model along with the coupling of the induced flux density obtained from the vector potential calculation, after the post-processing stage.

The tasks performed under each stage have been subdivided into different computer-aided engineering softwares for simplification of roles. In figure 4 it is possible to visualize the process that occurs on each stage of the field problem approach and how they rigorously interact with each other from the geometry until the experimental process. The softwares used are MATLAB for geometry generation and export of parsed data, Gmsh (Christophe Geuzaine, 2009) and GetDP (Dular and Geuzaine, 2013) for finite element analysis.

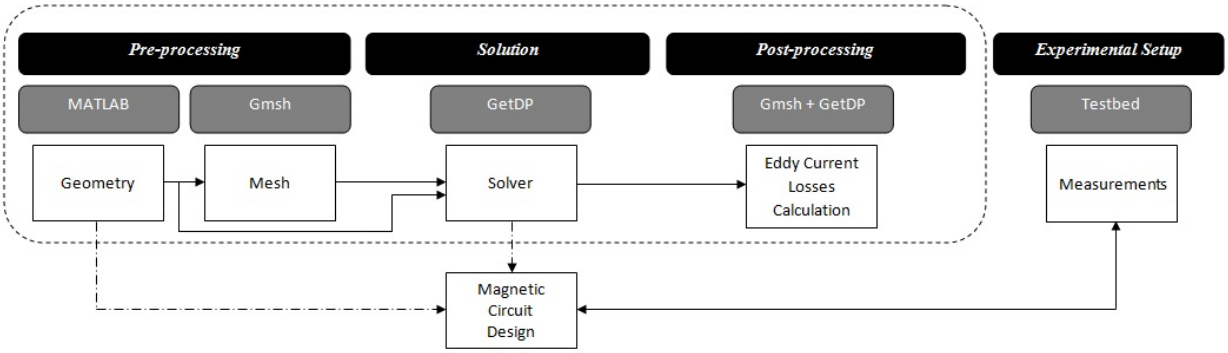

Figure 4: Process Stages

4.1 Pre-processing

The pre-processing tasks are divided into the generation of the geometry and the creation of a suitable mesh for the specific geometry to be studied. Morevoer, each task is assigned to a different CAE software.

The generation of a parametrized geometry is performed by MATLAB due to the flexibility, speed and language simplicity that the software provides. The geometry

to be constructed is based on the cross sectional area of a stack of laminated rings, hence, the basic rules of Euclidean geometry apply. In Figure 5 the steel stack is defined by the regions bounded by blue lines, while the impurity regions are bounded by red lines. The definition and indexing of the lines with respect to the coordinates and region declarations are fairly simple.

The input parameters used in MATLAB are:

- Number of sheets
- Lamination thickness
- Impurity layer thickness
- Mesh type
- Region definition
- Frequency
- Conductivity of the Material

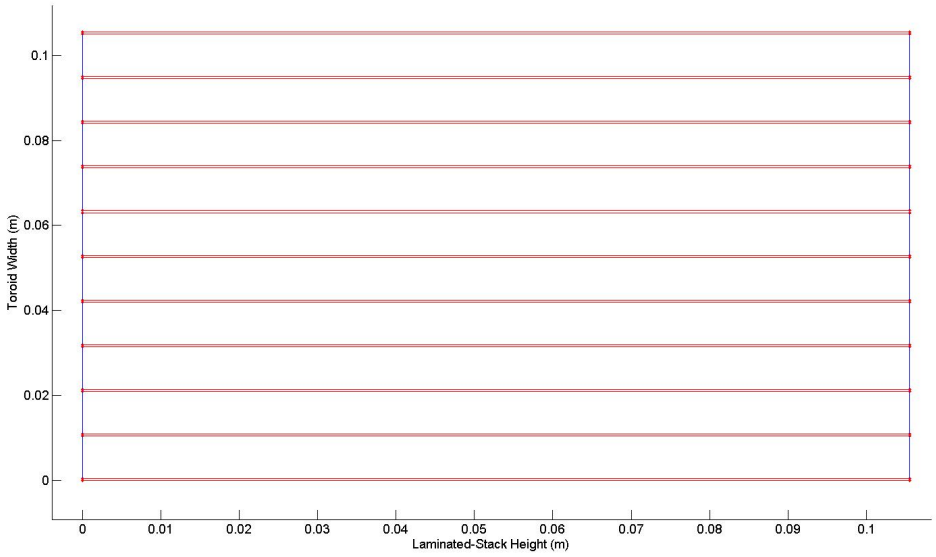

Figure 5: Cross Sectional Area of a Toroid using Matlab

Mesh type and region definition are two basic functions written to create a bridge between MATLAB and Gmsh. Mesh type is an option provided to choose between three types of mesh. The main purpose is to provide a suitable mesh for the given geometry to enhance computational time. The script developed in MATLAB allows the user to choose from two available static meshes (Figure 6), triangular and quadrangular, respectively, taking the inter-laminar surface thickness as a reference for

the element side length. This ensures a refined and uniform mesh throughout the whole region.

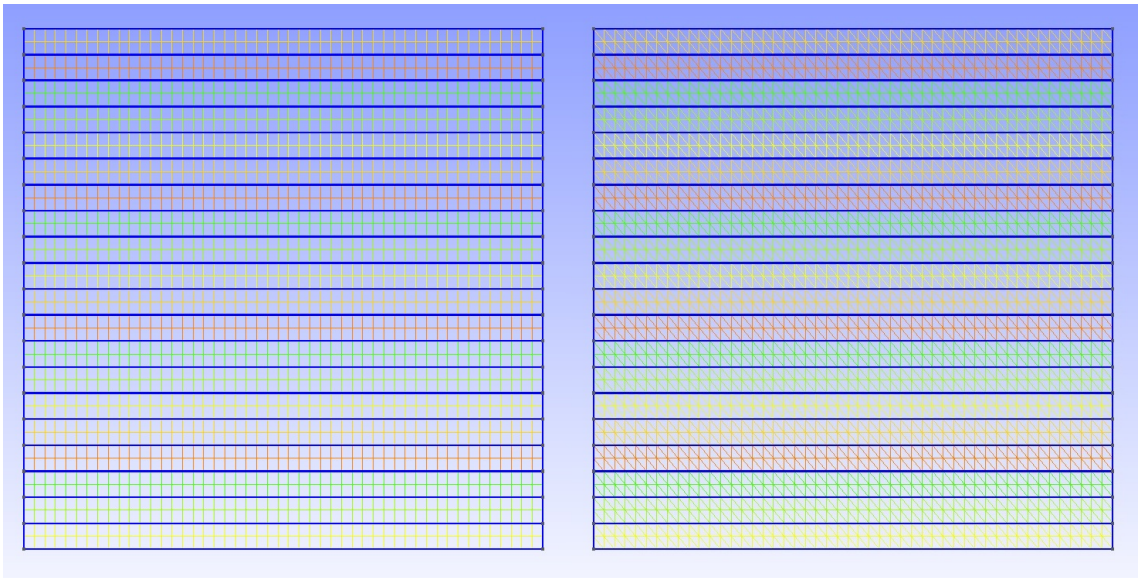

Figure 6: Static Meshing Example using Gmsh

Lastly, MATLAB exports a parsed text file using Gmsh's scripting language (i.e., .geo). Subsequently, Gmsh parses the information provided on the script and creates a mesh file (.msh) storing nodal coordinates, and indexing nodes and elements that will be required during the solution stage.

The mesh used throughout this thesis work is quadrangular as it computes faster while providing the same accuracy for the solution as the triangular mesh. The reason is that for the triangular mesh, although we have the same amount of nodes, the amount of elements is doubled, and the integration of each of them needs to be taken into account in the final computational time.

4.2 Solution

The solution stage is mainly carried out by GetDP, which is a software environment for the numerical solution of integro-differential equations. This software allows the coupling of multiple physical problems as well as offering a variety of numerical methods to choose from, including finite element method, boundary element method and volume integral methods. Unlike Gmsh, GetDP does not have a user interface, although, it can be run from Gmsh's GUI platform. However, to enhance computational speed it is recommended to run both programs (Gmsh and GetDP) from the command prompt. Since both programs are meant to compliment each other, no external scripts need to be written. GetDP also has its own scripting language and can be written as a regular ASCII text file.

GetDP's scripting language has been structured as block sets. The file contains the problem definition and can be summarized in eight block declaration stages. A brief description of each stage will be presented, post-processing and post-operation, will be described in the post-processing section. See appendix.

Group

Gmsh generates the input file required by GetDP, a mesh file. This mesh file identifies and indexes nodal coordinates, number of elements, type of element, region to which the element belongs, etc. In other words, the Group scripting block is in charge of identifying topological entities found in the mesh file. For this reason this is the first block that GetDP requires to be able to run any type of formulation. The geometry MATLAB script has been developed to identify each region and exports them as a text file that can be incorporated into the main solver.

Owing to the simple parametrized geometry created for the study of eddy current losses in uninsulated laminations during this thesis work, two major regions are declared: iron and impurities. Each region can be subdivided as well, giving the flexibility to study other test cases depending on the parameters given during the geometry generation, in the region definition section of the pre-processing stage.

Function

Geometrical entities are identified and classified, hence, global and piecewise continuous expressions must be assigned to the corresponding groups. This section will interact directly with the formulation block and piecewise continuous quantities such as magnetic permeability of the material, electric conductivity, etc. are introduced here. It is also possible to declare constants such as frequency or parameters required to perform time-stepping, specially for the study of nonlinear materials. Due to the interaction between the function block and the formulation block, it is possible to couple the magnetic properties of a certain material (i.e., B-H curve) and the calculation of the vector potential by using interpolation schemes, such as the Akima interpolation. Moreover, this block allows linearization of functions using Newton's method or functional iterations (Picard iteration). The formulation block uses the Garlekin space-discretization scheme, therefore, the equation needs to be linear with respect to the vector of 'Degree of freedom'(Dof).The Dof is defined in the formulation block and defines a vector of discrete quantities and it is used to establish a clear difference between the already computed quantities and unknown quantities (i.e.,Dof).

Constraint

Following the declaration of global and local quantities, the boundary conditions of the given geometry are defined, which will be read only once as the script is initialized. The boundary conditions may be defined in terms of the normal and

tangential field components. In our case-study and due to the flexibility of GetDP, the script can initialize the external boundary as a known constant, by assuming uniformly-distributed field strength along borders of the stack, hence defining a Dirichlet boundary condition. The boundary conditions of the cross section of a stack of laminations, can be either defined as a set of Dirichlet conditions or as a combination of Dirichlet and Neumann boundary conditions as periodic boundaries apply to the studied region. A set of Dirichlet conditions are declared as time-dependent function along the boundary and secondly a initialization value for the internal region, that will only be evaluated once during the calculations. Diversifying the set of conditions and adding a Neumann boundary condition allows us to use the symmetry of the given region to create periodic boundaries. This will enhance the computational time as, a quarter of the geometry may be used to calculate the vector potential and GetDP is able to define links between the degrees of freedom in the constrained region with the ones in the reference region, hence the mapping translating the geometrical elements from one region into the other.

Function Space

The function space is directly associated with the definition of a (or multiple) basis function and the already defined constraints. The most basic function space is the nodal finite element space, which is defined by the nodal functions over a certain domain, obtained from the mesh file. In other words, it is possible to construct the nodal basis function, also known as the shape functions of our finite element model, as a scalar field function as shown in (3.36) and (3.42). The function space will also be associated with the type association between the mapping from a vector space and its scalar field. For this thesis work we implemented a linear functional (Form1) linear map, perpendicular to the $-z$ plane, i.e. perpendicular curl-conforming field. In other words, the basis function is associated with the edges of the elements of opposite nodes. Essentially, whenever elements within a mesh share the same edge, the edge function is ensured to be tangentially continuous.

Jacobian

Jacobian refers to the general generation of methods for solving computational integral terms and for coordinate transformation of the reference elements. The definition is fairly standard in all cases and mainly depends on the dimension in which the problem is studied, 1-D, 2-D or 3-D.

Integration

In the same fashion as in the Jacobian section, the integration is referred to the Formulation and Post-processing blocks and is defined in a standard manner for most problems. This part of the script allows the implementation of multiple numerical or analytical integration methods, most commonly seen Gauss integration. In this section, it is possible to set the amount of integration points for each element type.

Formulation

The formulation is the core of GetDP's solver script as it interconnects all the aforementioned defined quantities (local, global) to a global equation. This is done by the declaration of arguments that are used in associated functions declared in other sections of the script, such as the Function block, Jacobian block, etc. Moreover, the formulation section allows the user to write the equations in their weak form, as shown in (3.35), which simplifies the code and increases flexibility in declaring math operators such as partial derivatives or curl, among others.

Considering the electric vector potential formulation (3.26) for modeling eddy currents we may consider $\nabla\Omega$ as a negligible factor. In electrical machines, the rotor's (bulk or laminated steel) net current is zero, therefore, $\nabla\Omega$ tends to zero and may be neglected in the formulation. Hence, the electric vector potential equals the magnetic field strength and equation (3.26) can be rewritten as

$$\nabla \times \frac{\nabla \times \boldsymbol{T}}{\sigma} - \frac{\partial \mu_{non}\, \boldsymbol{T}}{\partial t} - \frac{\partial \mu_{lin}\, \boldsymbol{T}}{\partial t} = 0 \tag{4.1}$$

As we observe in 4.1 a new term arises as the permeability in the inter-laminar region is assumed to be linear, while the permeability of the sheet is considered non-linear and it is solved by iteration.

The derivation of the expression of the electric vector formulation will be shown below by substituting the electric field and flux density variables within the equation

$$\nabla \times \frac{\nabla \times \boldsymbol{H}}{\sigma} - \frac{\partial \boldsymbol{B}}{\partial t} = 0 \tag{4.2}$$

In Table 1 GetDP expressions are displayed and their general counterpart, for syntax unification in the definition of electric vector potential formulation.

Table 1: GetDP Syntax Comparison

General	*GetDP*
H_n^k	$Dof\{H\}$
H_n^{k-1}	$\{H\}$
H_{n-1}	$\{H_{prev}\}$
Δt	$\$DTime$

The time derivative needs to be implemented in the function block, as the derivative (see equation 3.26) includes the local variable (permeability) and as mentioned before, Garlekin's method in GetDP does not allow nonlinear operations in the formulation block. Hence, the syntax displayed in Table 1 includes the terms addressed to n and k which refer to the timestep and iteration index, respectively.

Since the a linear map of the type 1-form has been declared , the function space is already associated with a curl operator and the curl operator of the expression to the left may be neglected in the formulation. The weak form formulation can be rewritten as follows

$$\int_{\Omega} \frac{1}{\sigma}(\nabla \times w) \cdot (\nabla \times H_n^k)\mathrm{d}\Omega + \int_{\Omega} w \cdot \frac{B(H_n^{k-1}) - B(H_{n-1})}{\Delta t}\mathrm{d}\Omega = 0 \tag{4.3}$$

The study of ferromagnetic materials forces us to rely on iteration methods. For this particular case as previously explained, the Newton-Raphson method has been implemented. Equation (4.3) must be rewritten in similar fashion to equation (3.55), hence, the Jacobian matrix can be calculated. For visualization purposes (3.44), (3.45), (3.46) will be rewritten as

$$S = \int_{\Omega} \frac{1}{\sigma}(\nabla \times w) \cdot (\nabla \times H_n^k)\mathrm{d}\Omega \tag{4.4}$$

$$D = \int_{\Omega} w \cdot [B(H_n^{k-1}) - B(H_{n-1})]\mathrm{d}\Omega \tag{4.5}$$

Although, equations (4.4)and (4.5) are not expressed as linear combinations associated with the nodal shape functions, Garlekin's method will be applied and both, the actual function and the weight function will be calculated in terms of the nodal values by GetDP, ensuring that the integration will be performed over the whole geometry. For simplicity the equation can now be expressed in matrix form, the residual as shown in equation (3.55) and the Jacobian matrix will be calculated in the same fashion as shown in equation (3.58).

The Jacobian matrix can be calculated quite easily by GetDP's embedded function JacNL, which ensures that the Dof term will be defined as an unknown value and that it needs to be calculated during each iteration as the partial differentiation with respect to the electric vector potential (i.e., $\frac{\partial}{\partial u}$). Redefining the nodal function-expressions as vectors, we express them as follows

$$\boldsymbol{N}_i = \boldsymbol{N} = \begin{bmatrix} N_1 \\ \cdot \\ \cdot \\ N_m \end{bmatrix} \tag{4.6}$$

$$\boldsymbol{N}_j = \boldsymbol{N}^T \tag{4.7}$$

Beginning from the general expression obtained in equation (3.58) we may rewrite the Jacobian matrix as

$$\frac{\partial \boldsymbol{r}(\boldsymbol{u})}{\partial \boldsymbol{u}} = \boldsymbol{S} + \frac{1}{\Delta t}\boldsymbol{D} + \frac{1}{\Delta t}\frac{\partial}{\partial \boldsymbol{u}}\left(\int_{\Omega} \boldsymbol{N}\mu\boldsymbol{N}^T\boldsymbol{u}\mathrm{d}\Omega\right) \tag{4.8}$$

As we know, the electric vector potential can be consider as equal to the magnetic field strength, which can also be expressed as a linear combination using the established notation used in (4.6) and(4.7)

$$\boldsymbol{H} = \boldsymbol{N}^T \boldsymbol{u} \tag{4.9}$$

Hence, substituting (4.9) into (4.8)

$$\frac{\partial \boldsymbol{r}(\boldsymbol{u})}{\partial \boldsymbol{u}} = \boldsymbol{S} + \frac{1}{\Delta t}\boldsymbol{D} + \frac{1}{\Delta t}\frac{\partial}{\partial \boldsymbol{u}}(\int_{\Omega} \boldsymbol{N}\boldsymbol{B}\mathrm{d}\Omega) \tag{4.10}$$

Taking the derivative with respect to the electric vector potential and using the mathematical properties of partial differentiation expansion

$$\frac{\partial \boldsymbol{r}(\boldsymbol{u})}{\partial \boldsymbol{u}} = \boldsymbol{S} + \frac{1}{\Delta t}\boldsymbol{D} + \frac{1}{\Delta t}\int_{\Omega} \boldsymbol{N}\frac{\partial \boldsymbol{B}}{\partial \boldsymbol{H}}\frac{\partial \boldsymbol{H}}{\partial \boldsymbol{u}}\mathrm{d}\Omega \tag{4.11}$$

Finally, we obtain a suitable Jacobian matrix expression that describes the behavior of the finite element model with respect to the $B-H$ magnetization curve, which can be used for the studies of eddy current losses and also for the study of losses in hysteric materials.

$$\frac{\partial \boldsymbol{r}(\boldsymbol{u})}{\partial \boldsymbol{u}} = \boldsymbol{S} + \frac{1}{\Delta t}\boldsymbol{D} + \frac{1}{\Delta t}\int_{\Omega} \boldsymbol{N}\frac{\partial \boldsymbol{B}}{\partial \boldsymbol{H}}\boldsymbol{N}^T\mathrm{d}\Omega \tag{4.12}$$

As we previously showed, the S and D matrix can be defined on GetDP as purely field related expressions and for this reason the furthermost term to the right can be rewritten as a function of only the partial derivative of the magnetic flux density in terms of the magnetic field strength $\frac{\partial \boldsymbol{B}}{\partial \boldsymbol{H}}$. Hence, in GetDP Newton-Raphson using the electric vector potential formulation for modeling eddy currents can be expressed

$$\begin{aligned}\int_{\Omega} \frac{1}{\sigma}(\nabla \times w)\cdot(\nabla \times H_n^k)\mathrm{d}\Omega + \frac{1}{\Delta t}\int_{\Omega} w\cdot[B(H_n^{k-1}) - B(H_{n-1})]\mathrm{d}\Omega + \\ \frac{1}{\Delta t}\int_{\Omega} w\cdot\frac{\partial B(H_n^{k-1})}{\partial H_n^{k-1}}\mathrm{d}\Omega = 0\end{aligned} \tag{4.13}$$

Resolution

The resolution is in charge of the construction of systems of equations suitable to the parameters defined in previous blocks. Hence, if the studies performed are based on time-harmonic solution or time stepping, these must be called in this block. For instance it is common to declare epsilon (for approximating to zero residual), the relaxation factor and the maximum amount of iterations in the case of time stepping in this section.

4.3 Post-processing

The post-processing can be performed by GetDP alone or as a combination of GetDP and Gmsh. The latest one allowing the interaction with Gmsh's graphical interface. However, this application is optional as the results can be extracted from the command prompt. Furthermore, the post-processing can be computed as part of the solver script, hence, two more stage-blocks need to be coded in the solver script: post-processing and post-operation.

Post-processing

After the solution of the field problem has been obtained, the eddy current losses may be calculated and the adequate integration schemes over the region can be applied.

The eddy current losses can be calculated by integrating the absolute value of the current density squared over the conductivity of the material, integrated over the region. To obtain the losses as W/kg we divide the calculated losses by the density of the material.

$$P_{eddy} = \frac{\int_\Omega \frac{|\boldsymbol{J}|^2}{\sigma} \mathrm{d}\Omega}{\rho_{Fe}} \tag{4.14}$$

The general equation for eddy current losses describes the integration over the region. This region should be extrapolated to the volume of the toroid so that the losses are coupled to a possible physical model. The toroid's volume can be calculated as a triple integral, depending on the height, the angle and the radius, in the same fashion as a cylinder.

$$\int_h \int_\theta \int_R [f(R,\theta,h)R] \mathrm{d}R \, \mathrm{d}\theta \, \mathrm{d}h \tag{4.15}$$

Substituting the integral over the region Ω by a triple integral describing the dimensions of physical model and being consistent in the definition of the domain as shown in Figure 5, we obtain

$$\int_0^x \int_0^{2\pi} \int_0^y \frac{|\boldsymbol{J}|^2 (y+r)}{\sigma m} \mathrm{d}R \, \mathrm{d}\theta \, \mathrm{d}h \tag{4.16}$$

where r is the inner radius of the toroid, y is the height of the stack, and m the mass calculated from the volume and the density of the material.

Post-operation

Lastly, the post-operation stage allows the storage and manipulation of data with external or internal applications and the results will be displayed later in the corresponding section.

5 Magnetic Circuit Design

Due to time and resources constraints, the measurements will be postponed for later work. However, the design of the magnetic circuit to be used for the validation of the $T - \Omega$ Eddy-Current model explained throughout this thesis work is presented.

The losses obtained from the calculations performed in the post-processing stage must be compared to those losses measured from an experimental set-up. The design of a suitable magnetic equivalent circuit becomes essential.

In electric machines the rotor and stator are not physically connected and the rotor may be considered as an independent section of the machine. In synchronous machines (SM) the magnetic flux is induced by the flow of currents through coils wound on ferromagnetic materials and the rotor is commonly excited by an external DC field. Owing to the manufacturing costs, SM rotors are commonly assembled as stacks of steel laminations. Therefore, 1mm-sheet rings may be used for the purpose of assembling a magnetic circuit (Figure 1) that has similar characteristics as those of a SM cylindrical rotor.

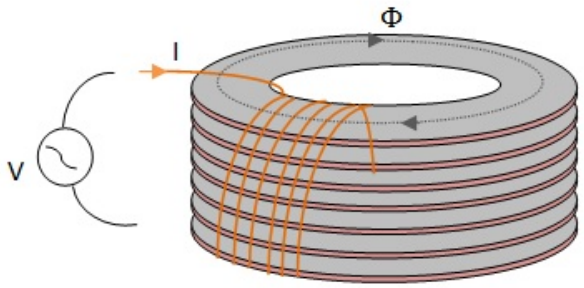

Figure 7: Toroid Representation

Inducing a magnetic flux into a magnetic material is associated to the relationship between the current-carrying conductor and the magnetic flux strength that it generates. Furthermore, the material properties play an important role as well, as the magnetic field strength value is directly proportional to the change in magnetic flux, i.e. $B - H$ curve of the material.

Experimental circuits are usually driven by voltage sources. However, whenever the desired induced flux is known, the rms voltage may be calculated but in order to achieve a constant flux across the material, the impedance of the coil needs to be studied and added to the calculated model, as this parameter depends on the change in temperature. Hence, the input voltage can be separated into two characteristic parameters (5.1): the voltage applied in the current-carrying conductor and the voltage induced on the iron.

$$U(t) = U_{Cu}(t) + U_{Fe}(t) \tag{5.1}$$

Expressing both voltages into their fundamental expressions, we obtained 5.2 and 5.3. The voltage induced in the iron depends on the change in magnetic flux within time, while the voltage induced in the coil depends on the variation of the input current and the resistance of the material.

$$U_{Fe}(t) = N\frac{\partial\Phi(t)}{\partial t} \tag{5.2}$$

$$U_{Cu}(t) = I(t)R_{Cu} \tag{5.3}$$

The resistance of the material can be expressed the resistivity of the material times the ratio between the length and the cross sectional area of the coil.

$$R_{Cu} = \rho_{Cu}\frac{l_{Cu}}{A_{Cu}} \tag{5.4}$$

where the resistivity can be expressed as a temperature dependent value: T and a reference temperature T_0.

$$\rho_{Cu} = \rho_{Cu,T_0}[1 + \alpha_{Cu}(T - T_0)] \tag{5.5}$$

The voltage U_{Fe} and U_{Cu} can be studied separately however, they are directly linked to the properties of the material. Applying Ampere's circuital law, it is possible to obtain the expression of the magnetomotive force (mmf), which is directly proportional to the number of turns around the lamination stack. For safety and accuracy purposes it is recommended to limit the current density across any coil, for which a value of 5.5 A/mm^2 has been selected. Assuming uniform current distribution, due to the high conductivity values of copper, the line current enclosed by the conductor can be also calculated from the integral of the current density over a finite cross sectional area.

$$I(t) = \frac{H(B)\, l_m}{N} \tag{5.6}$$

where l_m is the length of the magnetic path and the magnetic field strength is a function of the induced flux density.

Under a current supplied magnetic circuit it is assumed that the current and magnetic field strength are sinusoidal, which implies the variation of the flux density curve shape

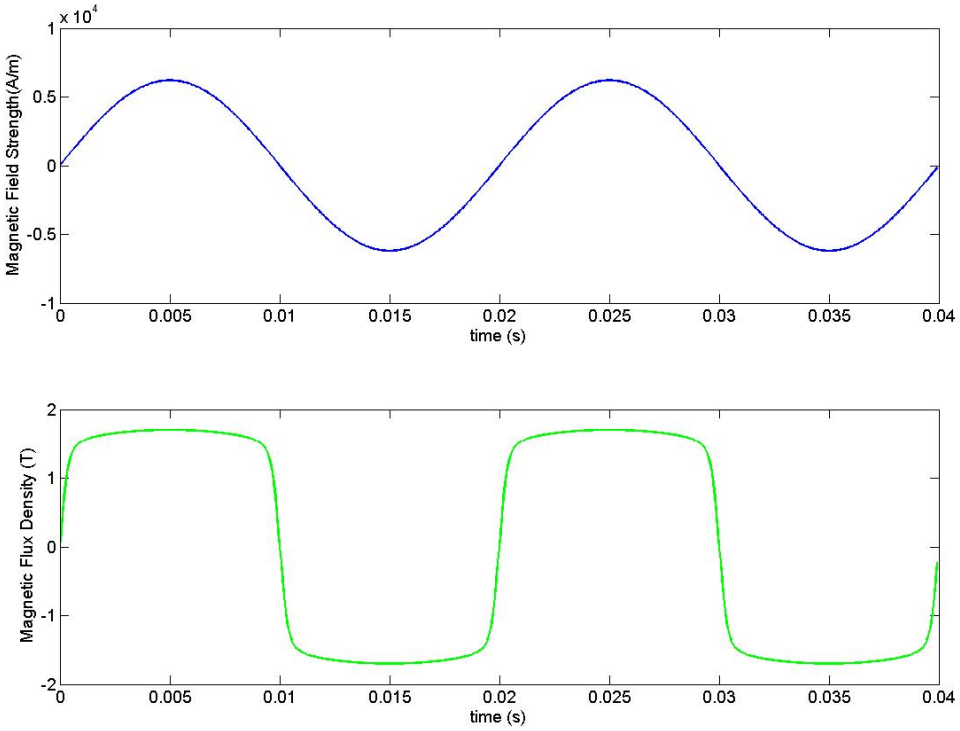

Figure 8: Sinusoidal Field Strength and Flux Density

Figure 8 shows the flux density curve obtained when the induced field is sinusoidal with a peak value of 6200 A/m at a frequency of 50 Hz for 2 cycles. The peak value of the flux density is estimated to be of 1.7 T and was obtained by interpolating the induced field with the material B-H curve displayed in Figure 9

The current can be approximated by limiting the current density of the coil over a the cross sectional area of the coil. Therefore, it is possible to obtain a general expression that relates the number of turns around the toroid to the desired peak current and the magnetic field strength obtained from the imposed magnetic flux.

$$N = \frac{Hl_m}{JA_{Cu}} \tag{5.7}$$

where A_{Cu} is calculated from the standarized wire gauge system: American wire gauge (AWG). In this manner it is possible ensure that the conductor is commer-

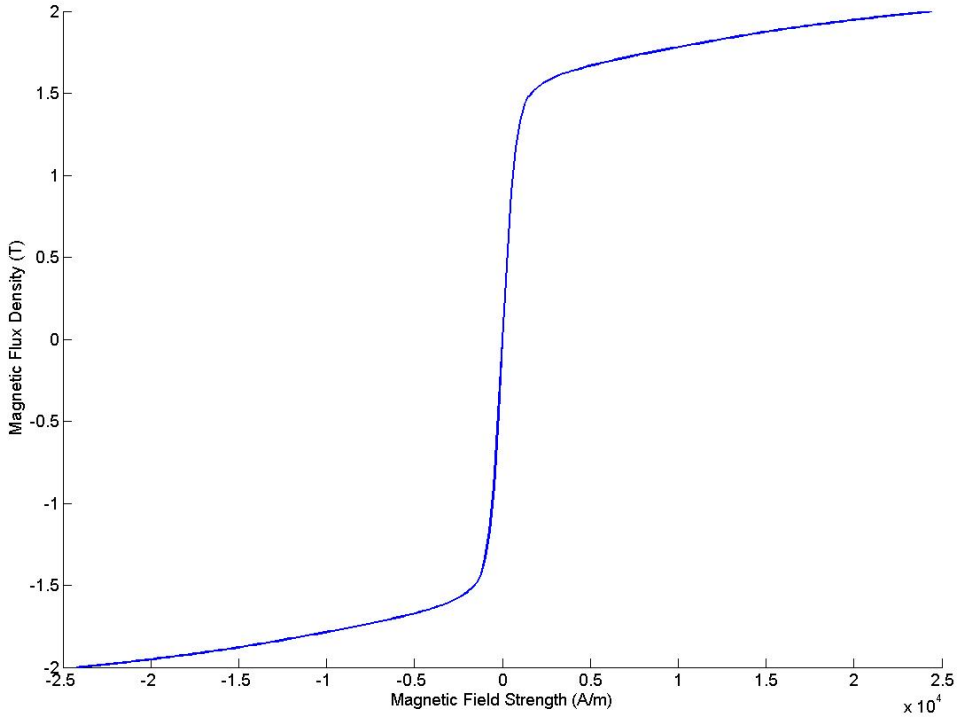

Figure 9: BH Curve

cially available off-shelf.

$$A_{Cu,AWG} = 0.012668mm^2\ 92^{\frac{36-AWG}{19.5}} \tag{5.8}$$

After obtaining the values of the desired peak flux density, the number of turns and the supplied current, equation 5.1 can be re-written as

$$U(t) = IR_{Cu} + N\omega AB \tag{5.9}$$

The number of turns and the thermal dependency of the resistivity of the copper may be added as well and the respective rms values for the input current and input voltage can be calculated.

$$U_{rms} = \frac{1}{\sqrt{2}} J\rho_{Cu,T_0}[1 + \alpha_{Cu}(T - T_0)]l_{Cu} + \frac{1}{\sqrt{2}} \frac{Hl_m\omega AB_p}{JA_{Cu}} \tag{5.10}$$

$$I_{rms} = \frac{I_p}{\sqrt{2}} \tag{5.11}$$

To ensure that the number of turns is feasible, and also ensuring a single layer of copper turns to maintain low flux leakage and capacitance between turns, the maximum amount of physical turns is calculated. This can be done by comparing the available area in the inner part of the ring to the area that the specific wire occupies.

$$N_{max} = \frac{A_{winding}}{A_{Cu}} = \frac{\pi(2rd_{Cu} - d_{Cu}^2)}{A_{Cu}} \tag{5.12}$$

where r, is the radius of the minor radius of the annulus and d_{Cu} corresponds to the diameter of the copper wire.

The design attempts to maintain a flux density peak value of 1.7 T, and the drop due to temperature rise is shown in figure 10. As we observe, the flux density drop is minimal under temperature between 20 and 100 degrees Celsius.

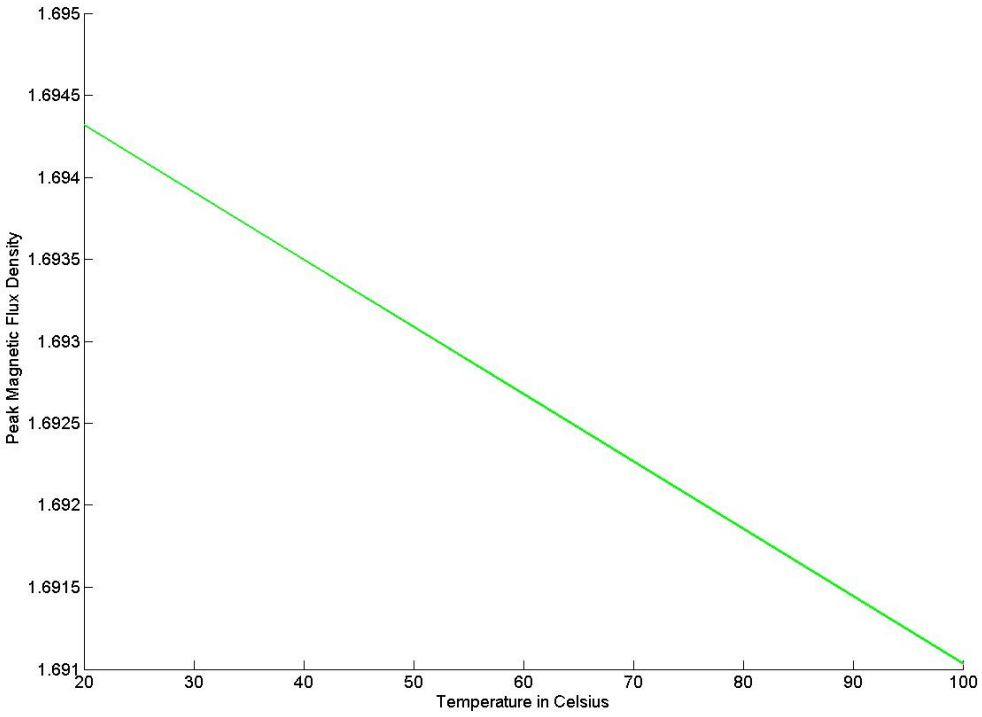

Figure 10: Flux Density vs. Temperature

Figure 11 summarizes the algorithm utilized in order to design the equivalent magnetic circuit designed for verification purposes. The algorithm requires the dimensions of the toroid, the wire gauge, the frequency, the peak flux density and the properties of the specific material used, i.e. B-H curve. The spline interpolation allows the calculation of new values of the magnetic field strength due to the induced field. The comparison of areas between the conductor's cross sectional area and the toroid's surface area, it is possible to determine the maximum amount of turns that such dimensions physically allow. Substituting Gauss's law of induction and the line integral of the current density over the surface area of the conductor, it is possible to determine the number of turns needed to obtain the desired field. The values of the maximum amount of turns N_{max} and the calculated number of turns N are compared to ensure that the number of turns needed to achieve the desired induced flux will be less or equal than the maximum number of turns that can be physically implemented. In this fashion we guarantee that the amount of turns is feasible for such dimensions. Furthermore, limiting the area populated by the conductors reduces end winding effects and capacitance between each turn. Whenever the requirement is met, a base voltage value is calculated and as the power supply is a voltage source, the currents need to be re-calculated for the variation in temperature, as the resistance of the conductor is temperature-dependent. The current is limited so that the impact on the desired flux is low as ultimately it is sought to impose a constant flux across the toroid. If the number of turns criteria fails, the script loops to find the most optimal gauge size for the specific application.

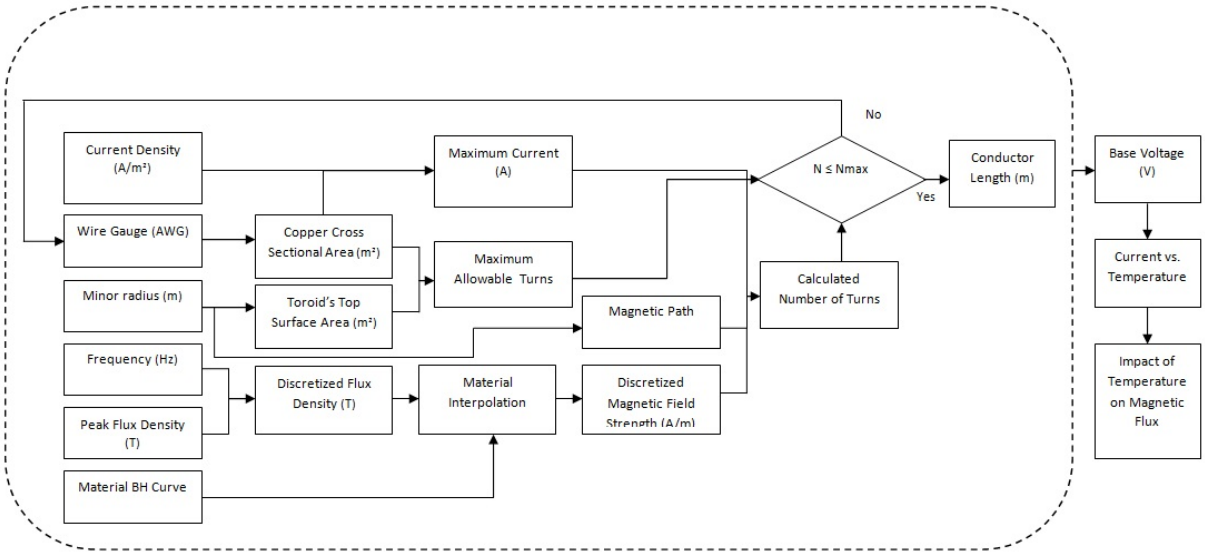

Figure 11: Magnetic Circuit Design Algorithm

Table 2: Magnetic Circuit Design Parameters

Frequency (Hz)	50
Surface Field (A/m)	6200
RMS Voltage (V)	77
RMS Current (A)	8
Number of Turns	510
Inner Radius (cm)	14
Outter Radius (cm)	16

Finally the values obtained throughout the design stages of the toroid are displayed in table 2

6 Numerical Model Verification

The calculations performed in the numerical model implemented in GetDP were verified by comparing its results to those of an analytical model implemented in MATLAB.

The study of inter-laminar conductivity leads to the geometrical definition of very thin layers in the micro-meter range. The ratio between the thickness of these inter-laminar regions to their height, defined by the height of the lamination stack, can be considered as infinite. For this reason, the verification was performed by comparing the results to the 1-D analytical loss model and subsequently in a more comprehensive manner, the 2-D model.

The validation of the numerical model was carried using the following parameters

Table 3: Validation Parameters

Number of Nodes	9801
Number of Elements	9996
Frequency (Hz)	1000
Conductivity (MS/m)	8.5
Relative Permeability	1000
Surface Field (A/m)	1200

The physical dimensions used in the 1-D analytical model were 0.5 mm x 10 cm, while in the 2-D case a 1 mm x 1 mm area was used.

6.1 1-D Analytical Model

Although, the numerical model and analytical model serve as a tool to study the field problem in a 2-D geometry, the losses obtained can be approximated to the ones in a 1-D model. The 1-D lamination model states that when the ratio between the thickness and the height of a lamination is extremely large, the edge effects are negligible and the solution of the diffusion equation in 1-D describes the field solution quite accurately Mayergoyz et al. (1984),Vecchio (1982). As shown in Figure 12 and Figure 13, even if the field is meant to be uniformly distributed along the edges of our geometry, it seems to be predominant only in one direction.

Evidently, if the height is in the y-direction and the thickness in the x-direction, then the eddy currents will be predominant in the y-direction and the impact of the x-component of the eddy currents can be neglected (Figure 14), considering no return path in our calculations.

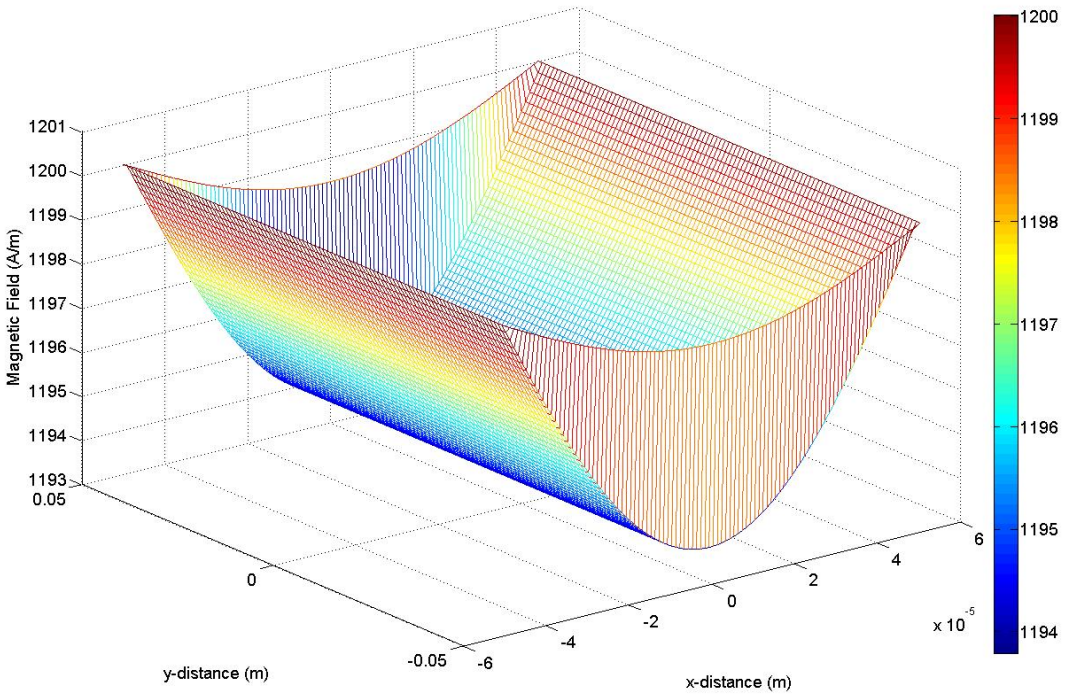

Figure 12: Field Strength Penetration within the Thickness of a Lamination

Under the previously mentioned assumptions, the eddy-current losses were calculated using the following analytical expression presented by Lammeraner and Stafl (1966)

$$P_{1D} = \frac{B_m^2 \sigma \omega^2 b^2 \rho_{Fe}}{6} F(\zeta) \tag{6.1}$$

where,$F(\zeta)$ is the skin effect factor and Bm is the mean value of the flux density. These parameters can be calculated explicitly as

$$F(\zeta) = \frac{3}{\zeta} \frac{\sinh(\zeta) - \sin(\zeta)}{\cosh(\zeta) - \cos(\zeta)} \tag{6.2}$$

$$B_m = 2\mu H_0 \frac{a}{2b} \sqrt{\frac{\cosh(\frac{2b}{a}) - \cos(\frac{2b}{a})}{\cosh(\frac{2b}{a}) + \cos(\frac{2b}{a})}} \tag{6.3}$$

H_0 is the field strength on the surface of the lamination and ζ is the ratio between the thickness of the lamination $2b$ and the depth of penetration a, i.e. $\zeta = \frac{2b}{a}$, where

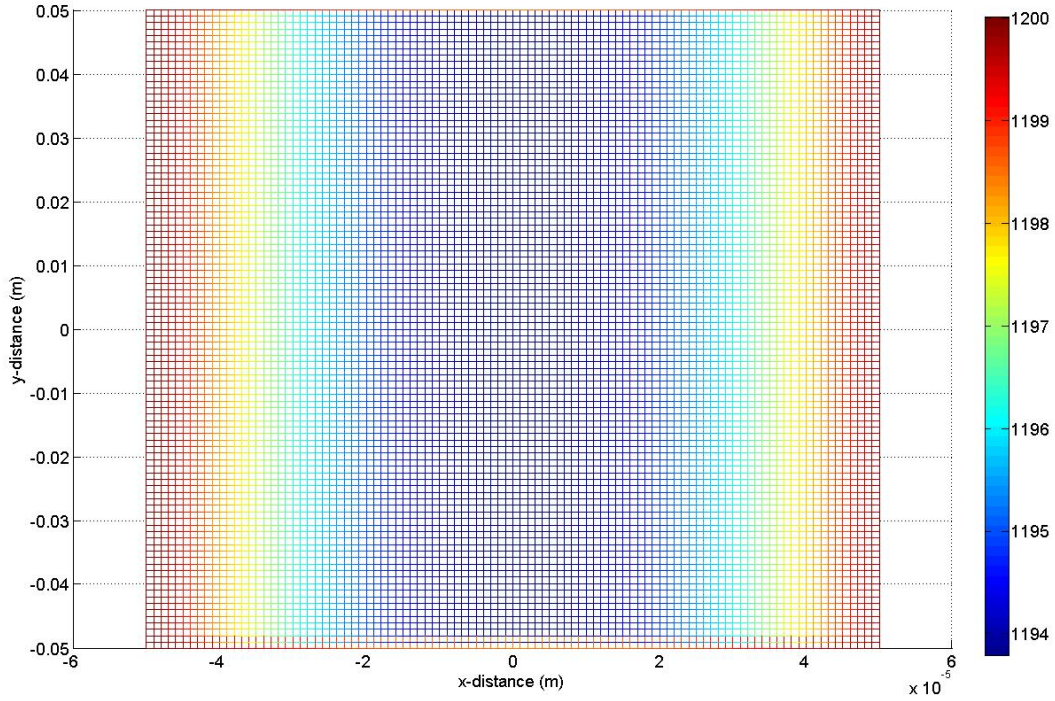

Figure 13: Field Strength Distribution XY Plane

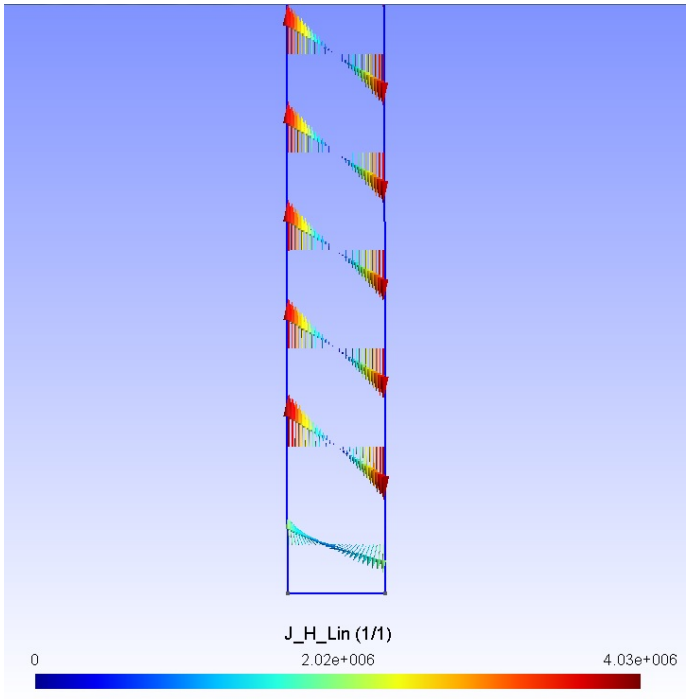

Figure 14: Vector Plot of Induced Eddy Currents

$$a = \sqrt{\frac{2}{\omega\sigma\mu}} \tag{6.4}$$

The 2D numerical estimated loss-model was compared to two different analytical models: the 1D model described by equation 6.1 and analytically integrating the current density in the 2D geometry as described in equation 4.14. In Figure 15 it is shown that the estimated eddy-current losses in both cases are fairly close, verifying that the numerical model is performing the desired calculations for thin inter-laminar layers.

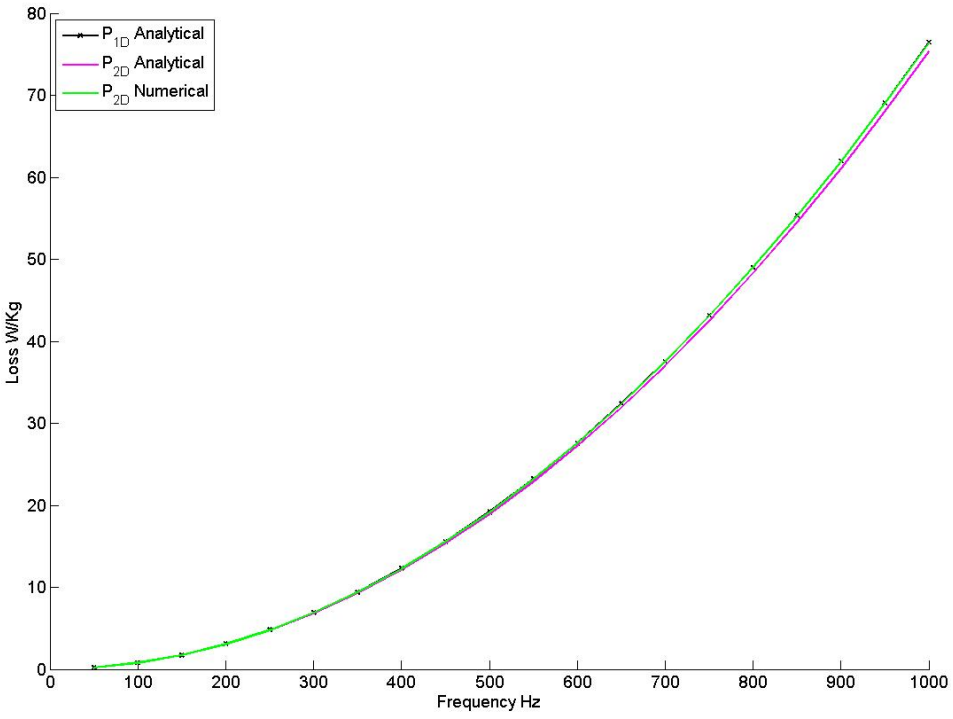

Figure 15: Eddy Current Losses vs Frequency

6.2 2-D Analytical Model

The 2-D analytical model of a current supplied problem is described by equation 6.5 where the source is assumed to be a constant magnetic field using the expression derived by Voipio (1987)

$$\begin{aligned} H_z = H_s \Bigg[& \frac{\cosh(\frac{1+j}{\sqrt{2}}\frac{x}{\delta})\cosh(\frac{1+j}{\sqrt{2}}\frac{y}{\delta})}{\cosh(\frac{1+j}{\sqrt{2}}\frac{a}{\delta})\cosh(\frac{1+j}{\sqrt{2}}\frac{b}{\delta})} \\ & + \sum_m \frac{\frac{4}{m\pi}\sin(\frac{m\pi}{2})}{1-j\left(\frac{m\pi\delta}{2a}\right)^2}\cos\left(\frac{m\pi x}{2a}\right)\frac{\cosh\left(\sqrt{2j+\left(\frac{m\pi\delta}{2a}\right)^2}\frac{y}{\delta}\right)}{\cosh\left(\sqrt{2j+\left(\frac{m\pi\delta}{2a}\right)^2}\frac{b}{\delta}\right)} \\ & + \sum_n \frac{\frac{4}{n\pi}\sin(\frac{n\pi}{2})}{1-j\left(\frac{n\pi\delta}{2b}\right)^2}\cos\left(\frac{n\pi y}{2b}\right)\frac{\cosh\left(\sqrt{2j+\left(\frac{n\pi\delta}{2b}\right)^2}\frac{x}{\delta}\right)}{\cosh\left(\sqrt{2j+\left(\frac{n\pi\delta}{2b}\right)^2}\frac{a}{\delta}\right)}\Bigg] \end{aligned} \tag{6.5}$$

Although, the equation describing the magnetic field in 2-D seems quite elaborate series form, we can write it in a more simplified form

$$H_z = H_s\big(H_{z0} + \sum H_{zm} + \sum H_{zn}\big) \tag{6.6}$$

This shows that the magnetic field is divided into 3 parameters: H_{z0}, H_{zm} and H_{zn}, i.e. initial value, field in x-direction and field in y-direction, all of them result of a product with the surface field strength. In Figure 16 we observe that the penetration of the field occurs from the edges into the middle of the lamination.

The losses were calculated analytically and numerically just as performed in the 1D loss model case. In the analytical calculation two methods of comparison were implemented. The first one is based on the integration over the current density divided by the conductivity of the material as shown in equation 4.14, which in Figure 17 is expressed as 'P_{2D} Analytical 1' and to ensure uniformity of results, the losses were also calculated using the Poynting Vector (equation 6.7) analytically, integrating over the edges of the region. The expression is presented in Figure 17 as 'P_{2D} Analytical 2'

$$S = \oint \boldsymbol{E} \times \boldsymbol{H} dl \tag{6.7}$$

The results displayed in Figure 17 seem to be consistent and the losses seem to be calculated accordingly.

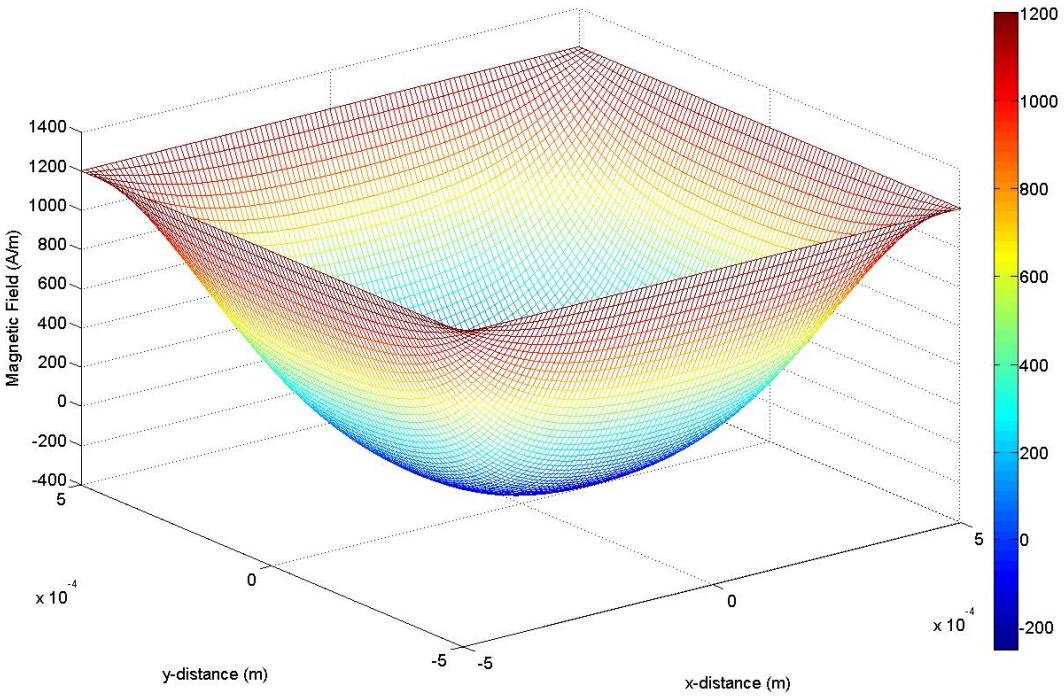

Figure 16: Field Strength Penetration within the Thickness of a Lamination in 2-D Analytical Model

6.3 Comparison of the Field Solution

To ensure consistency in our results the harmonic solution obtained by the calculation of the electric vector potential was compared to the solution obtained from the analytical expression 6.5.

A grid mesh was implemented in both models and selecting the same nodes on each, their solutions were compared. In Figure 18 we observe that the results for the imaginary and real part of the solution match quite accurately to the harmonic solution obtained in GetDP.

Furthermore, to ensure that the current densities were also properly calculated, the curl of the field 2-D model was taken (spatial derivative in 2-D).

The initial eddy currents are:

$$J_{x0} = \frac{H_s \cosh(\frac{1+j}{\sqrt{2}}\frac{x}{\delta})}{\cosh(\frac{1+j}{\sqrt{2}}\frac{a}{\delta})\cosh(\frac{1+j}{\sqrt{2}}\frac{b}{\delta})} \sinh\left(\frac{1+j}{\sqrt{2}}\frac{y}{\delta}\right)\frac{1+j}{\sqrt{2}\delta} \tag{6.8}$$

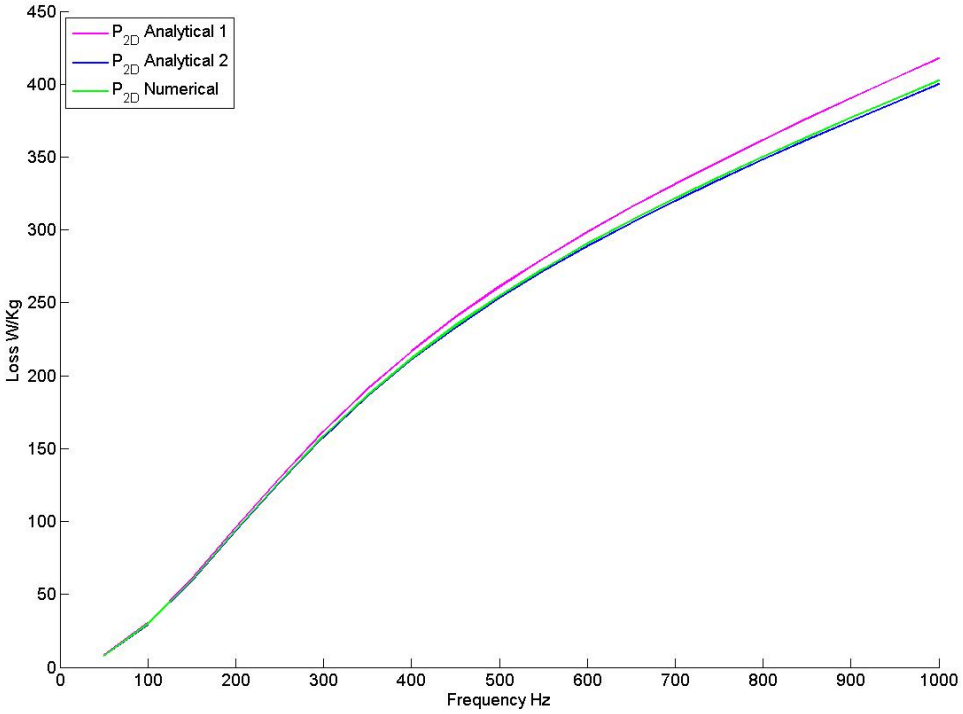

Figure 17: 1-D Model on a 2-D Plane

$$J_{y0} = \frac{H_s \cosh(\frac{1+j}{\sqrt{2}}\frac{y}{\delta})}{\cosh(\frac{1+j}{\sqrt{2}}\frac{a}{\delta})\cosh(\frac{1+j}{\sqrt{2}}\frac{b}{\delta})} \sinh\left(\frac{1+j}{\sqrt{2}}\frac{x}{\delta}\right)\frac{1+j}{\sqrt{2}\delta} \tag{6.9}$$

In the x-direction

$$J_{xm} = H_s \sum_m \left[\frac{\frac{4}{m\pi}\sin(\frac{m\pi}{2})\cos\left(\frac{m\pi x}{2a}\right)}{(1-j\left(\frac{m\pi\delta}{2a}\right)^2)\cosh\left(\sqrt{2j+\left(\frac{m\pi\delta}{2a}\right)^2}\frac{b}{\delta}\right)} \right. \tag{6.10}$$
$$\left. \sinh\left(\sqrt{2j+(\frac{m\pi\delta}{2a})^2}\frac{y}{\delta}\right)\frac{\sqrt{2j+\left(\frac{m\pi\delta}{2a}\right)^2}}{\delta}\right]$$

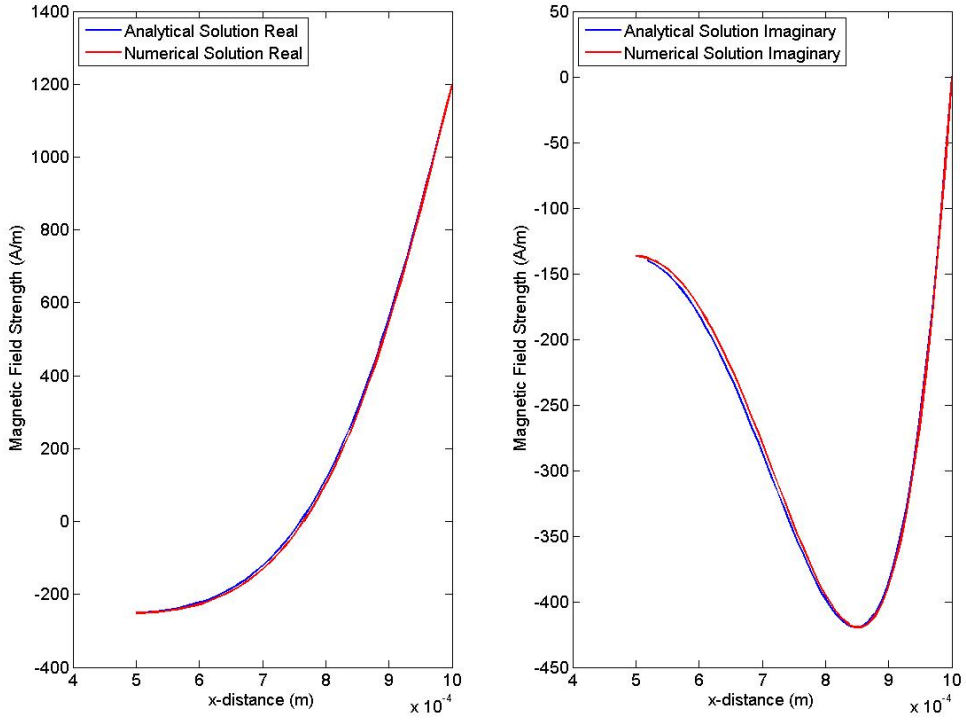

Figure 18: Verification of the Field Solution

$$J_{ym} = -H_s \sum_m \frac{\frac{4}{m\pi}\sin(\frac{m\pi}{2})\cosh\left(\sqrt{2j+\left(\frac{m\pi\delta}{2a}\right)^2}\frac{y}{\delta}\right)}{(1-j\left(\frac{m\pi\delta}{2a}\right)^2)\cosh\left(\sqrt{2j+\left(\frac{m\pi\delta}{2a}\right)^2}\frac{b}{\delta}\right)}\sin\left(\frac{m\pi x}{2a}\right)\frac{m\pi}{2a} \tag{6.11}$$

In the y-direction

$$J_{xn} = -H_s \sum_n \frac{\frac{4}{n\pi}\sin(\frac{n\pi}{2})\cosh\left(\sqrt{2j+\left(\frac{n\pi\delta}{2a}\right)^2}\frac{x}{\delta}\right)}{(1-j\left(\frac{n\pi\delta}{2a}\right)^2)\cosh\left(\sqrt{2j+\left(\frac{n\pi\delta}{2a}\right)^2}\frac{b}{\delta}\right)}\sin\left(\frac{n\pi y}{2b}\right)\frac{n\pi}{2b} \tag{6.12}$$

$$J_{yn} = H_s \sum_n \left[\frac{\frac{4}{n\pi}\sin(\frac{n\pi}{2})\cos\left(\frac{n\pi y}{2b}\right)}{(1-j\left(\frac{n\pi\delta}{2b}\right)^2)\cosh\left(\sqrt{2j+\left(\frac{n\pi\delta}{2b}\right)^2}\frac{a}{\delta}\right)} \right. \\ \left. \sinh\left(\sqrt{2j+(\frac{n\pi\delta}{2b})^2}\frac{x}{\delta}\right)\frac{\sqrt{2j+\left(\frac{n\pi\delta}{2b}\right)^2}}{\delta} \right] \tag{6.13}$$

These results were plot and their real components in the x- and y- direction are shown in Figure 19

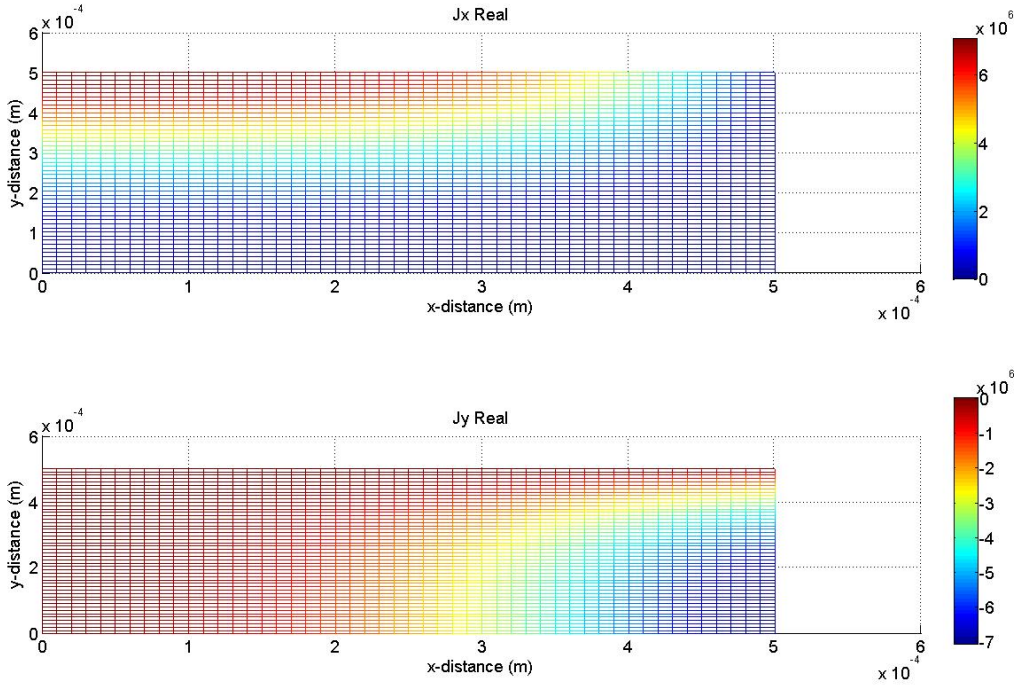

Figure 19: Eddy-current Real Component in x- and y-direction

In the same fashion the currents calculated in the analytical model were compared to the harmonic solution from the numerical model

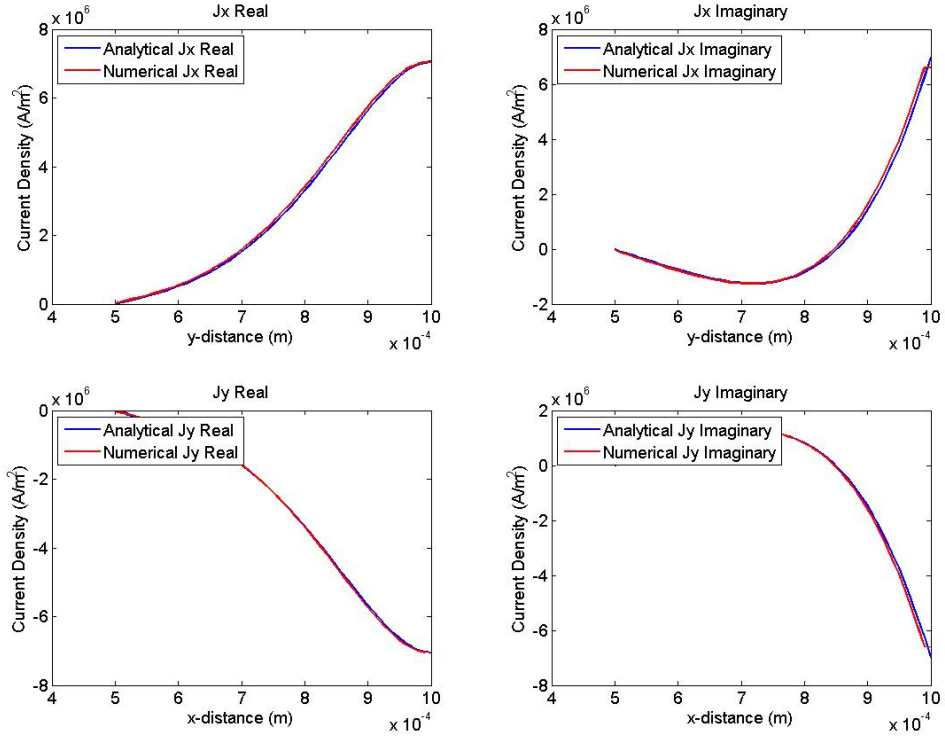

Figure 20: Comparison between the Analytical and Numerical Eddy-current Values

7 Results and Discussion

In this section the results of the studies performed will be displayed and discussed. The parameters used for the study of the eddy current losses in uninsulated laminated stacks are provided below in table 4 and table 5. Furthermore, the mesh parameters shown in table 5 were obtained by comparing the losses computed by using a very fine mesh.

Table 4: Study Parameters

Number of Sheets	20
Sheet Thickness (mm)	1
Inter-laminar Layer Width* (μm)	6 - 10
Frequency (Hz)	50 - 1000
Conductivity of Iron (MS/m)	8.5
Normal Inter-laminar Conductivity (MS/m)	8.5 - 0.0000085
Relative Permeability	1 - 1000
Surface Field (A/m)	6200

* Unless otherwise stated, the graphical representations displayed in the results section were obtained using a fixed inter-laminar width of 6 μm.

Table 5: Mesh Parameters

Element Type	Bi-linear
Element Order	First
Number of Nodes	28750
Number of Elements	29372
Integration Points	7

The elements include the sum of quadrangular elements and lines elements.

The problem solved is non-linear and the discretization in space and time are performed as shown in section 3.6 and their methods are displayed in table 6.

The calculation of the eddy current losses has been performed by integrating induced currents throughout the geometry. Applying the axi-symmetrical properties in the post-processing stage using cylindrical coordinates, as shown in equation 4.16, the losses in a toroid were calculated.

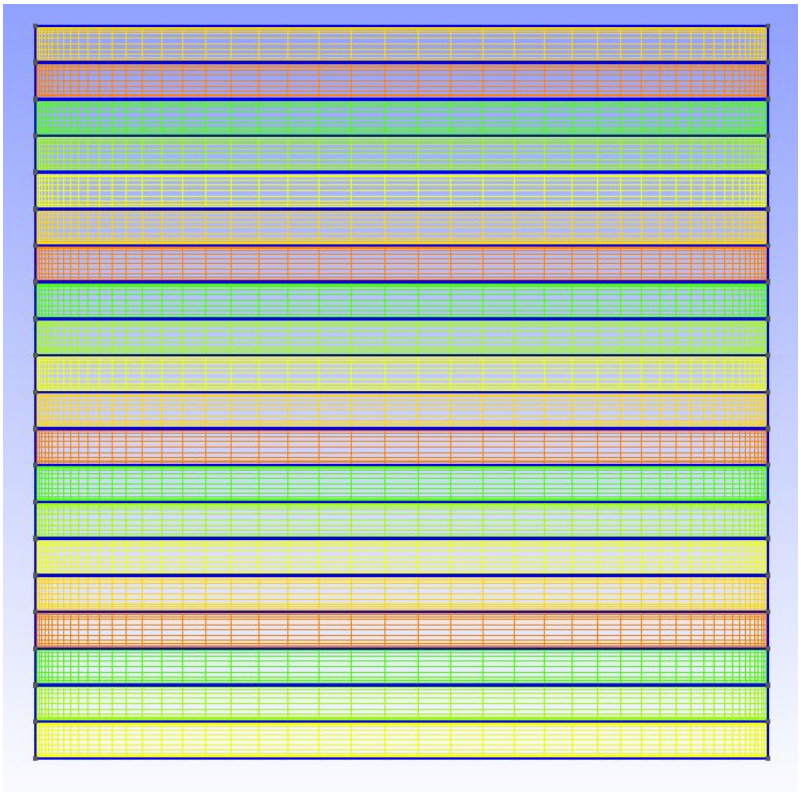

Figure 21: Mesh

Table 6: Discretization

Space Discretization	Garlekin Method
Time Discretization	Backward Euler Method
Time Steps	200
Periods	2

In the appendix section is presented the scripts to generate the studied geometry with an inter-laminar width of 6 μ and for the formulation.

7.1 Effect of Conductivity Degradation

The first study made was to observe the impact of conductivity degradation in the inter-laminar layer on the eddy current losses, over a fixed frequency range. The results are shown in Figures 22 and 23.

The degradation of the normal conductivity between layers causes an opposite effect as expected. Intuitively, it would be thought that as the inter-laminar conductivity decreases, smaller eddy-current-loops within the thickness of the lamination appear, similarly to the case of insulated laminated cores, decreasing the average losses. In Figure 22 we observe the losses increase as the conductivity decreases and behaves uniformly throughout the specified range of frequencies. The increase in losses occurs rather slowly. Whenever the laminar normal conductivity decreases to a value of 4%, from the initial conductivity of 8.5 MS/m, the increase in losses becomes evident.

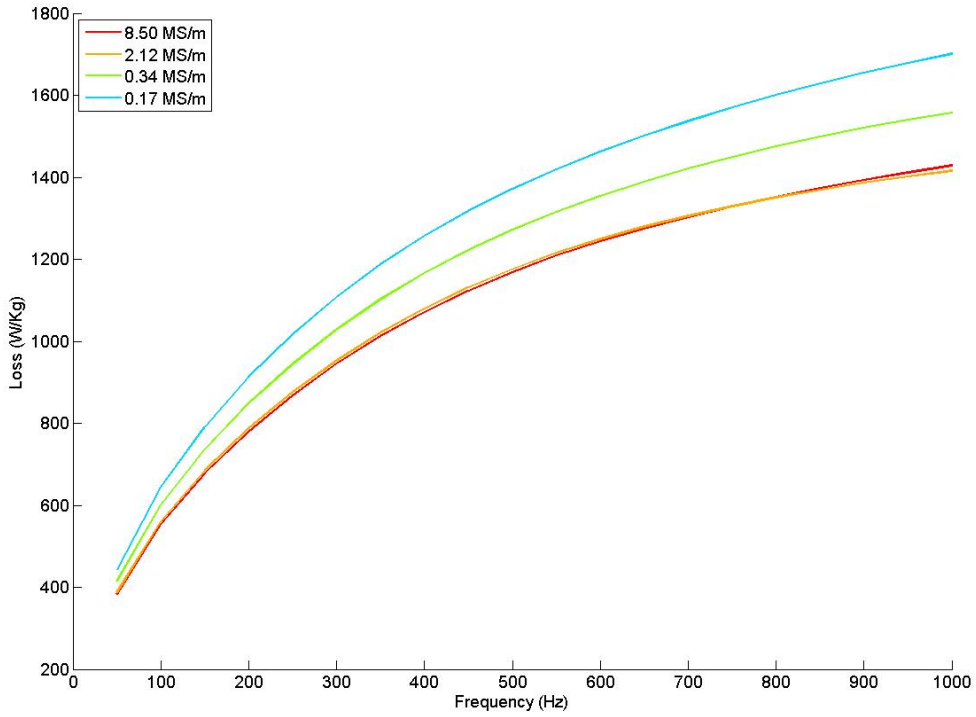

Figure 22: Loss vs. Frequency with High Conductivity for an Inter-laminar Layer

As observed, degradation of inter-laminar electrical conductivity increase the losses but it is not until it reaches values below 4% of the ideal conductivity of the sheet, when the increase of losses becomes dramatic. However, once the conductivity is quite low, for instance 8.5 S/m shown in Figure 23, the behavior of the losses become what was originally expected, hence, the losses decrease. This behavior occurs only for a range of frequencies as we see that the losses start increasing quite

rapidly again.

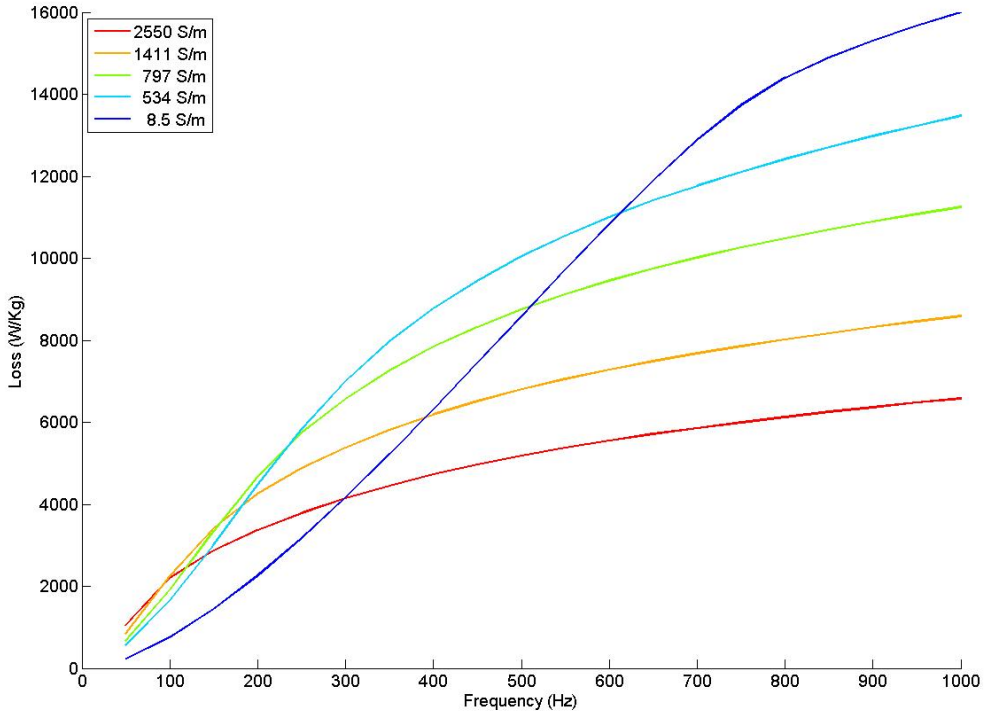

Figure 23: Loss vs. Frequency with Low Conductivity

7.2 Relative Permeability and Loss Calculation

The relative permeability was assumed to be linear in the inter-laminar area, while the permeability of the iron is nonlinear and calculated by interpolation, with the material characteristics. Furthermore, it was studied throughout a range between 1 and 1000, to study the impact of low and high permeability in the calculation of eddy current losses in uninsulated cores.

Losses seem to undergo dramatic changes under low inter-laminar conductivity conditions. For this reason it is important to ensure that the values calculated are as accurate as possible. The impact of high and low permeability need to be studied.

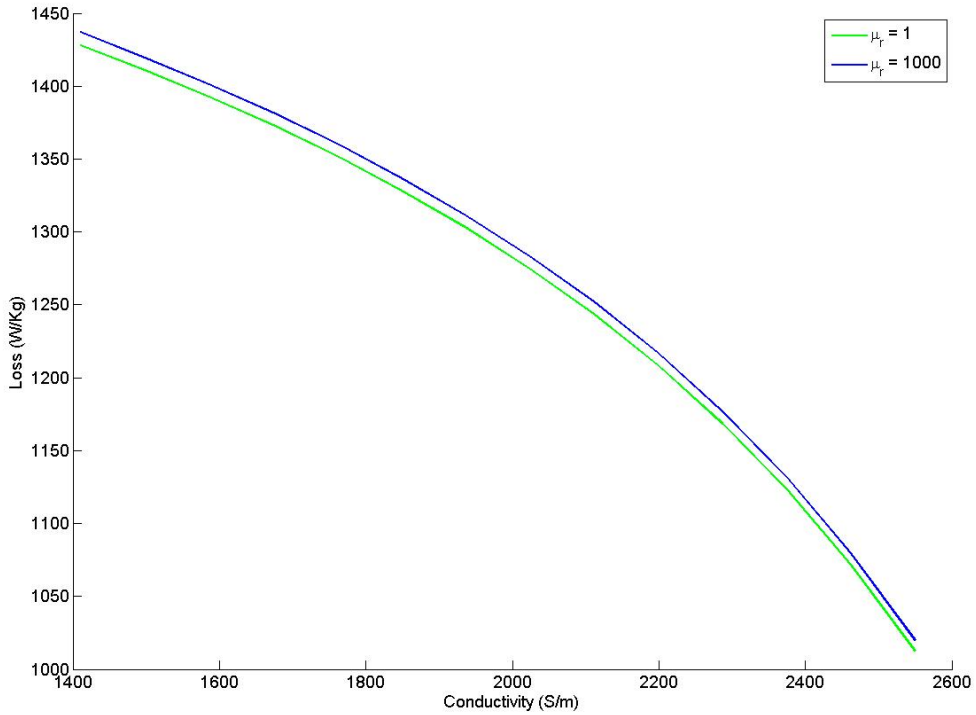

Figure 24: Loss vs. Low Conductivity at 50 Hz

In Figure 24 we are able to observe the eddy current losses calculated at a frequency of 50 Hz. As shown in the previous subsection, the losses increase due to the low conductivity normal to the lamination. The results obtained in both cases, low and high permeability, do not seem to vary much in terms of calculated losses. Furthermore, in Figure 25, the study shows that the relative difference in calculated losses is pretty low, for cases in which the conductivity is low and high and for frequencies of 50 Hz and 300 Hz.

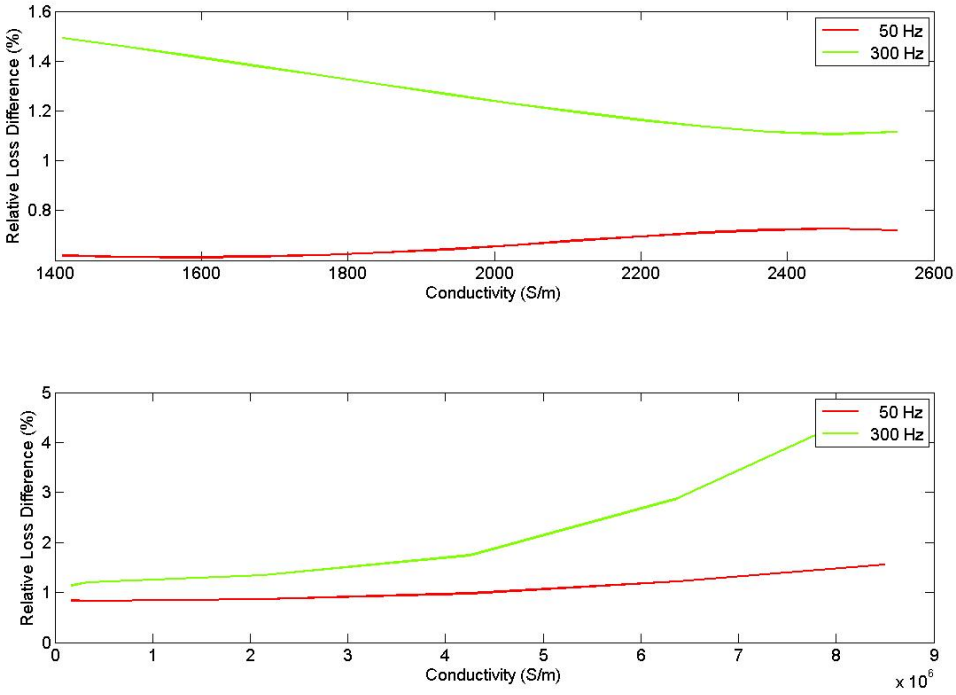

Figure 25: Relative Loss Difference

7.3 Inter-laminar Layer Width

The width was considered to be between 6 μm and 10 μm as these values are comparable to those used in insulated steel-sheets.

In Figures 26 and 27 we observe the impact of the width under low and high inter-laminar conductivity at 50 Hz and 300 Hz. This validates the study made before, as we observe that the losses at a frequency of 300 Hz are clearly higher at a conductivity of 8.5 S/m and vice versa, lower conductivities at higher values of conductivity seem to have greater losses. The losses caused by the width however is negligible as the scale remains almost unchanged for each studied case.

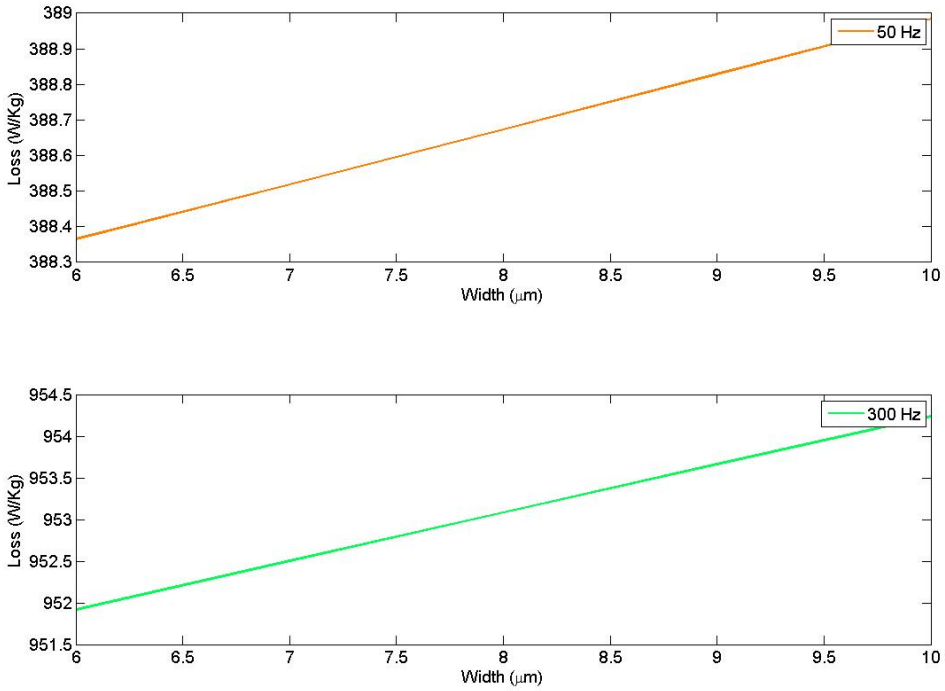

Figure 26: Loss vs. Width with Conductivity = 8.5 MS/m

The losses vs. frequency are shown in Figure 28-(a). This verifies that our model is consistent. The inter-laminar section in our model grows inwards, so in the ideal case where the iron and the normal laminar conductivity is the same, the losses will be the same independently from the thickness of the damaged layer.

In Figure 28-(b) the opposite case is shown, in the case of a normal conductivity of 8.5 S/m. As we observe, the width does not have a major impact on the eddy current losses in such a small range.

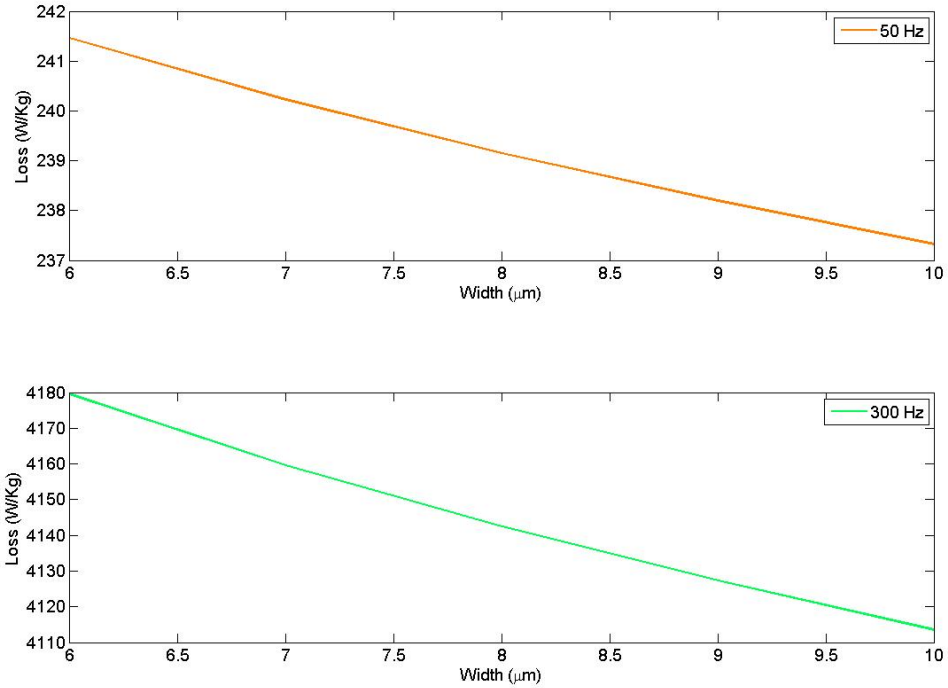

Figure 27: Loss vs. Width with Conductivity = 8.5 S/m

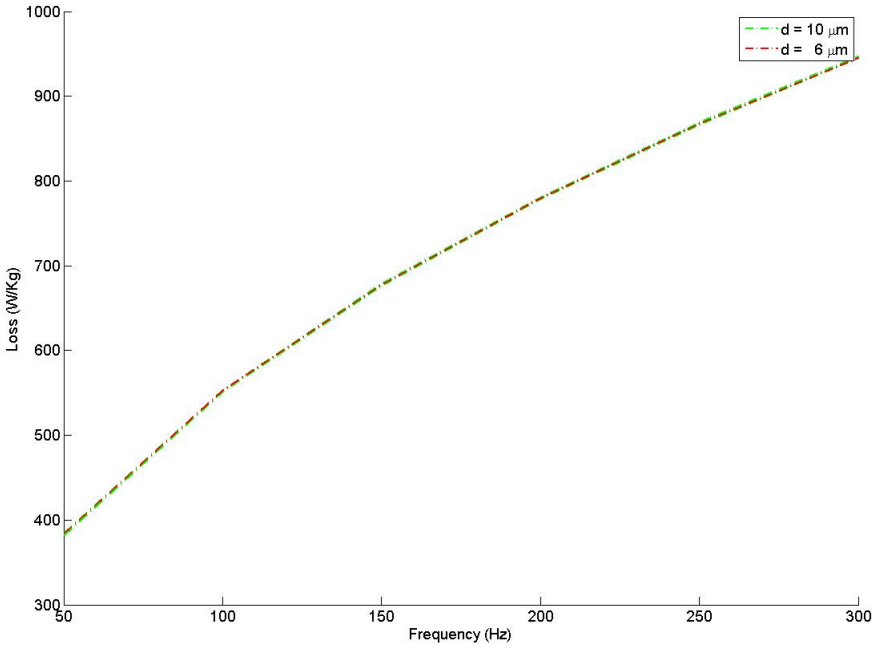

(a) Conductivity = 8.5 MS/m

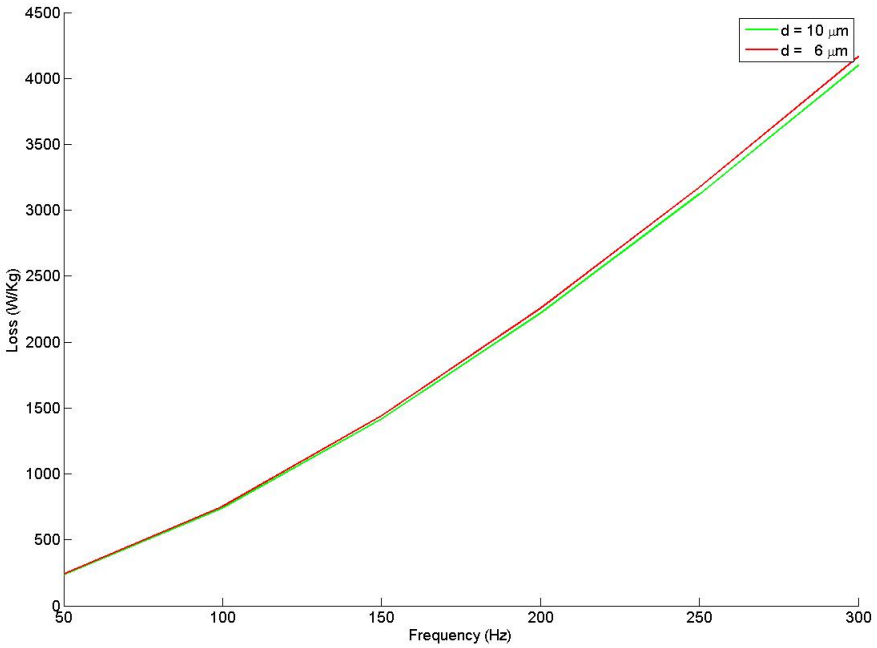

(b) Conductivity = 8.5 S/m

Figure 28: Loss vs. Frequency with Different Inter-laminar Conductivity

Lastly, a value of 2462 S/m in Figure 29 shows that at lower frequencies a smaller inter-laminar region generates more losses than a greater one.

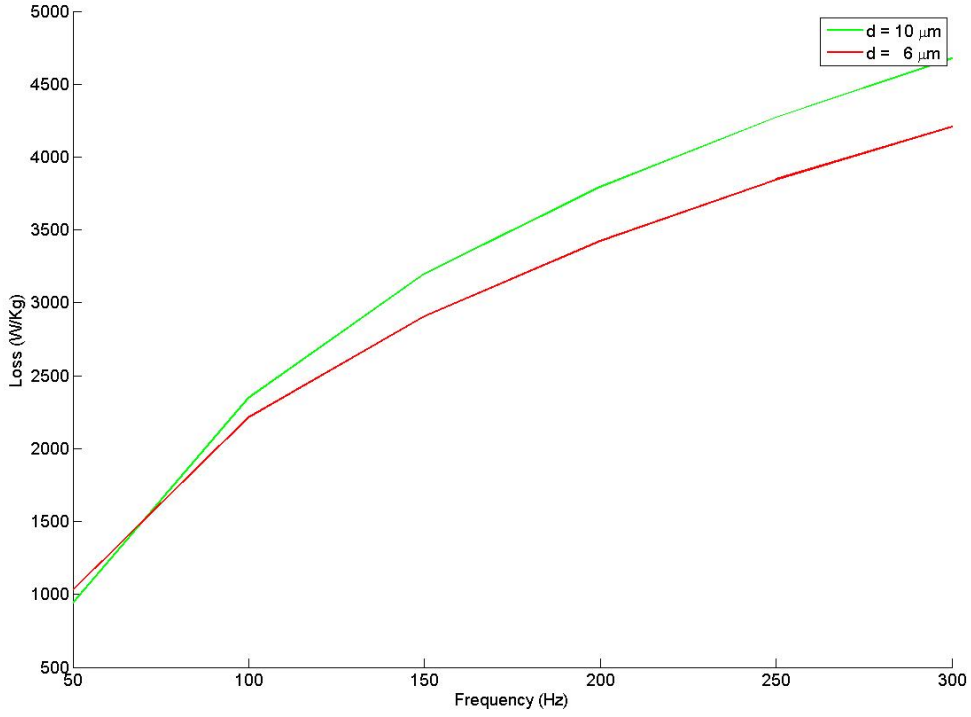

Figure 29: Loss vs. Frequency with Conductivity = 2462 S/m

7.4 Insulated vs. Uninsulated Laminated Stacks

Essentially, the results found in the previous subsection show that it is possible that insulated and uninsulated laminated cores behave similarly, confirming the results shown by Coombs et al. (2001).

The parameters used were the same as in the previous studies. The difference lays in the geometry. The uninsulated laminated core (Figure 30(b)), assumes that the damage caused by the manufacturing process grows inwards like in the case of scratches and oxide layers. On the contrary, the insulated stack model has insulation attached to the surface of the lamination (Figure 30(a)). To be consistent, the thickness of the lamination is 1 mm and the inter-laminar region widths are of 10 μm to ensure greater comparable differences, which maintains the same amount of iron in both cases.

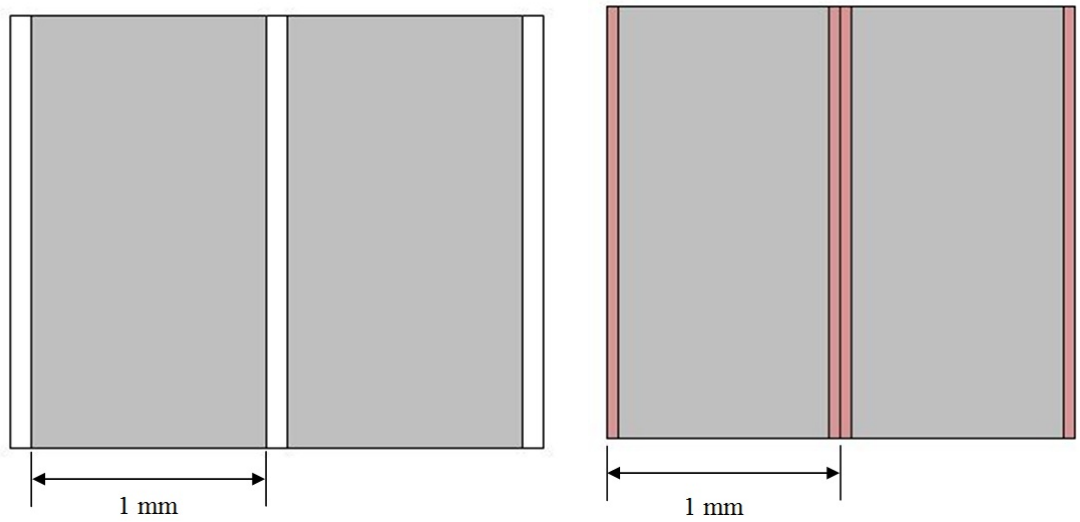

(a) Insulated (b) Uninsulated

Figure 30: Model Representation

The losses confirm the previously shown results. The losses seem to be lower at higher frequencies using uninsulated cores in comparison to the losses calculated in insulated laminated stacks and vice-versa as seen in Figure 31.

7.4.1 Cost Analysis

The aim of this work is to study the inter-laminar effects in uninsulated laminated steel-stacks. The results show that the use of uninsulated laminations can reduce losses at higher frequencies in comparison to the estimated losses found in insulated stacks. The increment of inter-laminar area also increases the induce voltages per turn (Bjerkan, 2005) and becomes more predominant at higher frequencies.

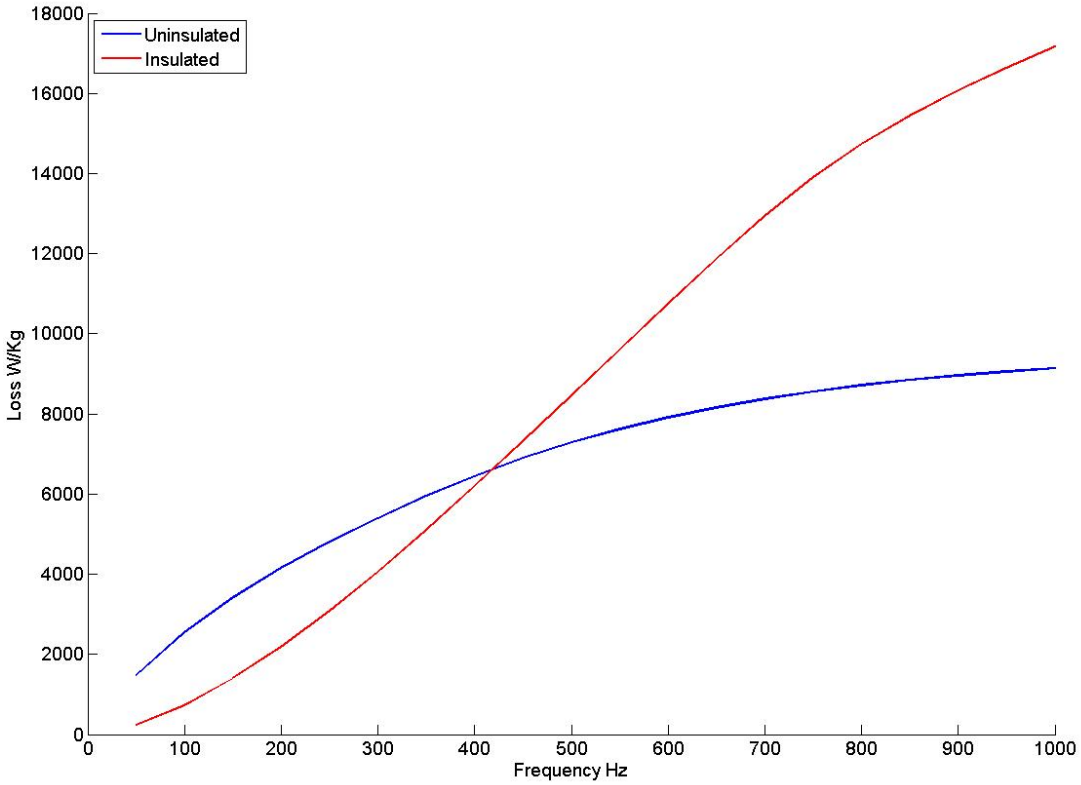

Figure 31: Loss vs. Frequency

Table 7: Electrical Steel Prices Year 2012

Uninsulated Steel (EU/ton)	680 - 950
Insulated Steel (EU/ton)	800 - 1100

In table 7 we observe the approximate range of prices as of year 2012. The price relative difference is approximately 15%.

The use of uninsulated steel in certain applications is clear not only on the technical side but also on the economical side. For example, if we take both of the upper number prices and calculate the difference it shows that we save only 150 Eur/ton, however, in the industry the amount of purchased electrical steel for the manufacturing of rotating electrical machines and transformers is quite large. If we assume hypothetically that a company purchases at least 10,000 ton/year, the savings are of about a 1,500,000 EU per year.

8 Conclusion

The degradation of conductivity on the surface of electrical steel is inevitable. Furtheremore, surface roughness is needed as the annealing performed during the stacking process may create micro-weldings between laminations, creating random current paths that would ultimately increase the losses. For this reason the normal conductivity (or resistivity) of laminated cores should be determined. This could provide enough information about the possible frequencies and applications at which the laminated core can operate.

If the permeability is constant in the inter-laminar layer, the loss calculation can be performed using low or high permeability values, as the relative difference is low. In the case of inter-laminar widths between 6 μm and 10 μm, the relative loss difference is negligible, for this reason it is recommended to use bigger inter-laminar regions as it enhances the convergence of the model.

The inter-laminar effects should be included in the calculation of losses in electrical machines and transformers as the impact is clearly far from negligible. The inclusion of the inter-laminar effects could not only contribute to the performance enhancement of machines but also has economical advantages. Insulated steel is more expensive than uninsulated electrical steel and as we have observed in the results section, at higher frequencies, uninsulated laminations generate lower losses than insulated ones, at higher frequencies, hence, uninsulated laminations could be used as a more economical alternative for certain applications.

References

Beckley, P. (2002). *Electrical Steels for rotating machines*. Institution of Electrical Engineers IET.

Bertotti, G. (1988). General properties of power losses in soft ferromagnetic materials. *Magnetics, IEEE Transactions on*, 24(1):621–630.

Bjerkan, E. (2005). *High Frequency Modeling of Power Transformers*. PhD thesis, Norwegian University of Science and Technology.

Christophe Geuzaine, J.-F. R. (2009). Gmsh: A 3-d finite element mesh generator with built-in pre- and post-processing facilities. *International Journal for Numerical Methods in Engineering*, 79(11):1309–1331.

Codecasa, L., Dular, P., Specogna, R., and Trevisan, F. (2010). A perturbation method for the geometric eddy-current formulation. *Magnetics, IEEE Transactions on*, 46(8):3045–3048.

Coombs, A., Lindenmo, M., Snell, D., and Power, D. (2001). Review of the types, properties, advantages, and latest developments in insulating coatings on nonoriented electrical steels. *Magnetics, IEEE Transactions on*, 37(1):544–557.

Dlala, E., B.-A. and Arkkio, A. (2008). Efficient magnetodynamic lamination model for two-dimensional field simulation of rotating electrical machines. *Elsevier Journal of Magnetism and Magnetic Materials*, 320:1006–1010.

Dular, P. and Geuzaine, C. (2013). GetDP reference manual: the documentation for GetDP, a general environment for the treatment of discrete problems. `http://www.geuz.org/getdp/`.

Hofmann, H. and Sander, S. (1998). High-speed synchronous reluctance machine with minimized rotor losses. In *Industry Applications Conference, 1998. Thirty-Third IAS Annual Meeting. The 1998 IEEE*, volume 1, pages 118–126 vol.1.

Keskinen, E. (1990). *Use of Electric Vector Potential in Finite Element Solution of Three Dimensional Eddy Current Problems*. PhD thesis, Helsinki University of Technology. Licenciate Thesis.

Kotiuga, P. (1987). On making cuts for magnetic scalar potentials in multiply connected regions. *Journal of Applied Physics*, 61(8):3916–3918.

Lammeraner, J. and Stafl, M. (1966). *Eddy Currents*. Iliffe Books LTD.

Luomi, J. (1993). *Finite Element Metods for Electrical Machines*. PhD thesis, Chalmers University of Technology. Lecture Notes.

Mayergoyz, I., Abdel Kader, F., and Emad, F. (1984). On penetration of electromagnetic fields into nonlinear conducting ferromagnetic media. *Journal of Applied Physics*, 55(3):618–629.

Mayergoyz, I. and Serpico, C. (1999). Nonlinear diffusion of electromagnetic fields and excess eddy current losses. *Journal of Applied Physics*, 85(8):4910–4912.

Menana, H. and Feliachi, M. (2011). An integro-differential model for 3-d eddy current computation in carbon fiber reinforced polymer composites. *Magnetics, IEEE Transactions on*, 47(4):756–763.

Nakata, T., Takahashi, N., Fujiwara, K., and Okada, Y. (1988). Improvements of the t- omega method for 3-d eddy current analysis. *IEEE Transactions on Magnetics*, 24:94–97.

Overshott, K., Preece, I., and Thompson, J. (1968). Magnetic properties of grain-oriented silicon iron. part 2: Basic experiments on the nature of the anomalous loss using an individual grain. *Electrical Engineers, Proceedings of the Institution of*, 115(12):1840–1845.

Pippuri, J. (2010). *Finite Element Analysis of Eddy Current Losses in Steel Laminations of Inverter-fed Electrical Machines*. PhD thesis, Helsinki University of Technology.

Ren, Z. (2002). T-omega; formulation for eddy-current problems in multiply connected regions. *Magnetics, IEEE Transactions on*, 38(2):557–560.

Tosaka, T., Nagano, I., Yagitani, S., and Yoshimura, Y. (2005). Determining the relative permeability and conductivity of thin materials. *Electromagnetic Compatibility, IEEE Transactions on*, 47(2):352–360.

Vecchio, R. (1982). The calculation of eddy current losses associated with rotating magnetic fields in thin laminations. *Magnetics, IEEE Transactions on*, 18(6):1707–1709.

Voipio, E. (1987). *Kenttteoria*. Otakustantamo.

Yating, Y., pingan, D., and Tuo, Y. (2011). Investigation on contribution of conductivity and permeability on electrical runout problem of eddy current displacement sensor. In *Instrumentation and Measurement Technology Conference (I2MTC), 2011 IEEE*, pages 1–5.

Zirka, S., Moroz, Y., Marketos, P., and Moses, A. (2010). Loss separation in nonoriented electrical steels. *Magnetics, IEEE Transactions on*, 46(2):286–289.

A Magnetization in Stack Model

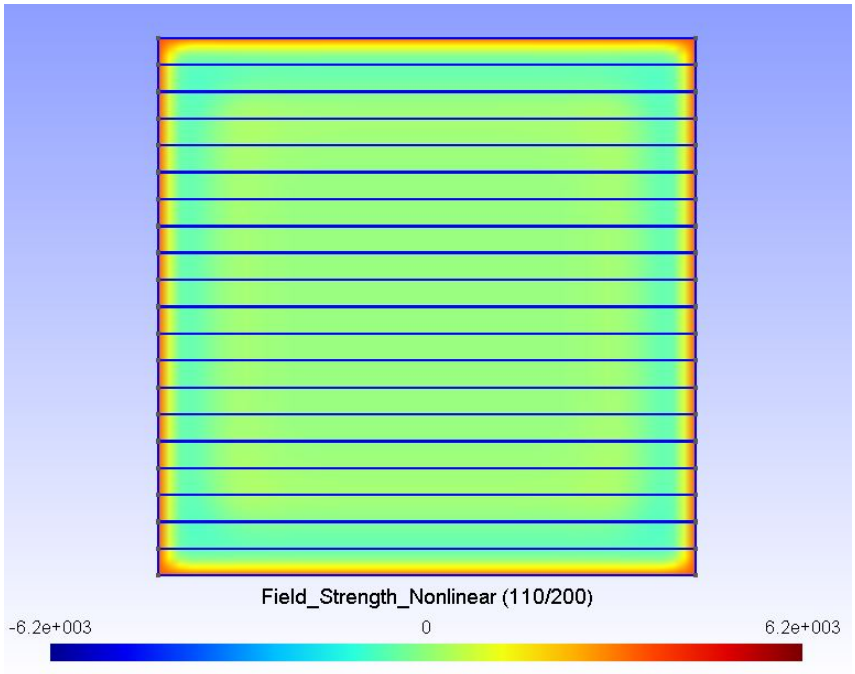

(a) Field Strength Distribution

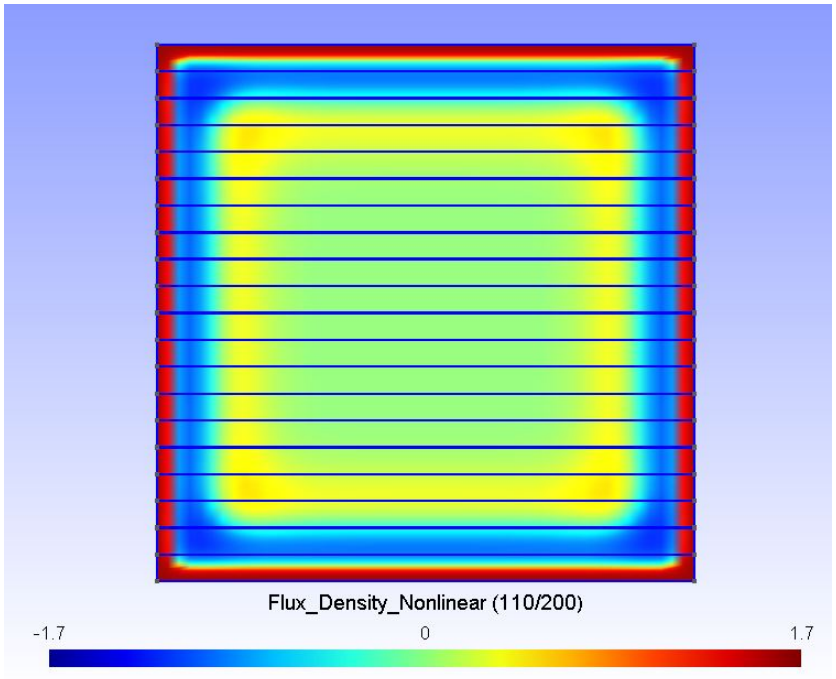

(b) Flux Density Distribution

Figure A1: Magnetization of Electrical-Steel Stack with $\sigma = 8.5$ MS/m

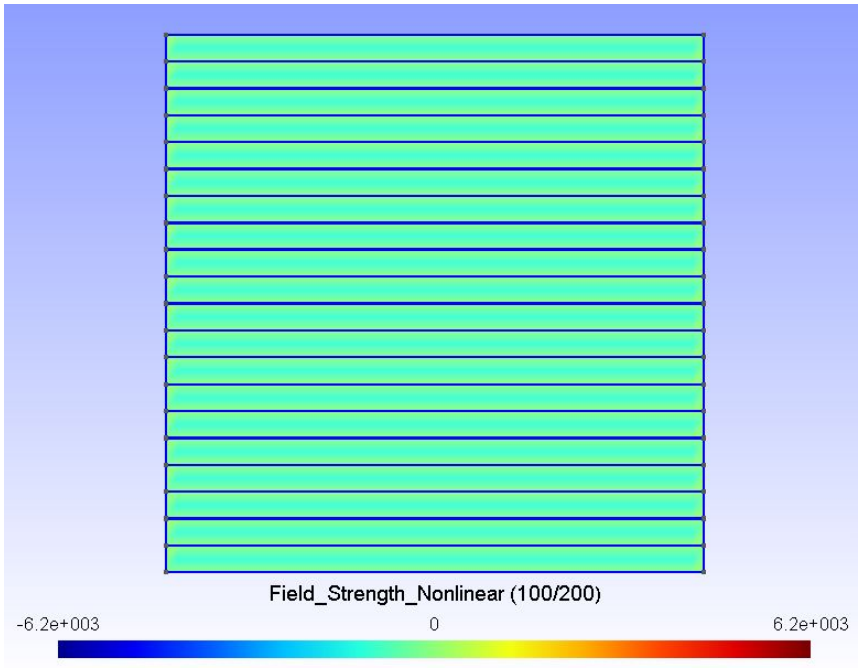

(a) Field Strength Distribution

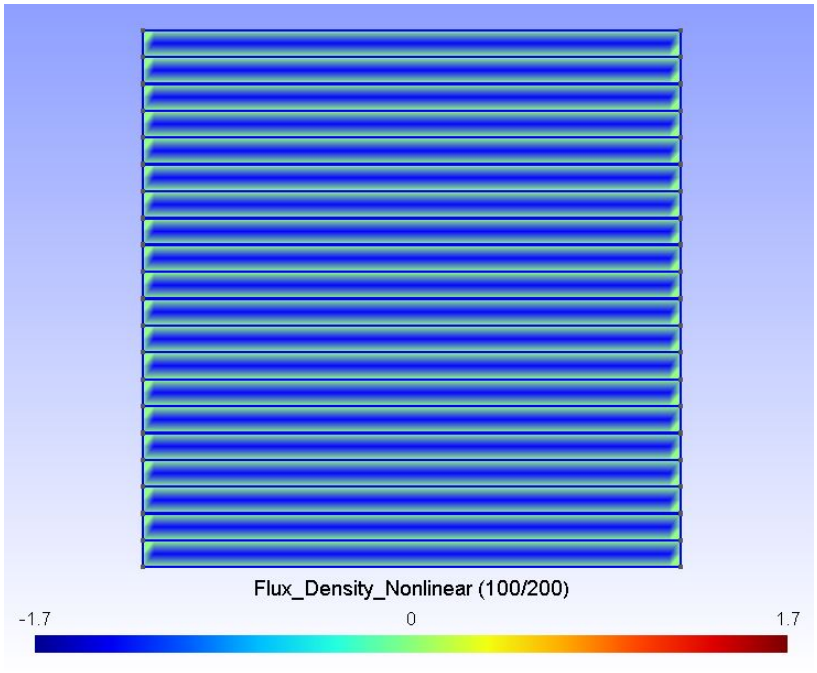

(b) Flux Density Distribution

Figure A2: Magnetization of Electrical-Steel Stack with $\sigma \approx 0$

B GetDP Script: Formulation

```
#include "GetDP_Material_mu.txt";

Group{

Iron = Region[208];
CSurface= Region[209]; /* Lamination Surface*/
EdgeBound= Region[207];     /* Boundary Line Around Geometry*/
Stack = Region[{Iron, CSurface}];
}


Function{
mu0 = 4*3.1415926*1e-7;
mur = 1000;
sig[Iron] = 8.5e6;       /* Conductivity of Iron*/
sig[CSurface] = 8.5e6;   /* Conductivity of Inter-laminar Layer*/

Freq = 50; Phase = 0.;
omega=2.*Pi*Freq;
TimeFct_ExtSin[] = F_Sin_wt_p [] {omega, Phase};

Periods = 2.0;
Nper = 200;
dt = Periods/(Freq*Nper);
tmax = Periods/Freq;

T_Time0 = 0.;
T_TimeMax = tmax;
T_DTime[] = dt;
T_Theta[] = 1.; /* Euler*/

mu_lin        =  mu0*mur;
    mu_non[Stack] = InterpolationAkima[Norm[$1]]{ListAlt[h_mat2, mu_mat2]};

dmudH [Stack] = dInterpolationAkima[Norm[$1]]{ListAlt[h_mat2, mu_mat2]};
B[Stack] = $1#2 * mu_non[#2];
    dBdH [Stack] = mu_non[$1]+Norm[$1]*dmudH[$1];

maxit = 100.;
relax = 1.;
eps   = 1e-6;

BC[] = 1200;  /* Linear Initial Boundary Condition*/
// BC[]  = 6200; /* Non-Linear Initial Boundary Condition*/

}


Constraint{
  { Name DirichletBoundaryCondition; Type Assign;
Case{
  {Region EdgeBound; Type Assign; TimeFunction TimeFct_ExtSin[]; Value BC[] ;}
    }
  }
  { Name InitializeBoundaryCondition; Type Assign;
Case{
  {Region Stack; Type Init; Value 0.0;}
    }
  }
}

FunctionSpace {
  { Name FunctSpA; Type Form1P;
    BasisFunction {
      { Name Hja; NameOfCoef Nja; Function  BF_PerpendicularEdge; Support Stack; Entity NodesOf[All]; }
}
```

```
    Constraint {
      {NameOfCoef Nja; EntityType NodesOf; NameOfConstraint DirichletBoundaryCondition; }
    }
  }
  { Name FunctSpB; Type Form1P;
    BasisFunction {
      { Name Hjb; NameOfCoef Njb; Function  BF_PerpendicularEdge; Support Stack; Entity NodesOf[All]; }
}
    Constraint {
      {NameOfCoef Njb; EntityType NodesOf; NameOfConstraint InitializeBoundaryCondition; }
    }
  }
}

Jacobian {
  { Name JMat ;
    Case {
      { Region All; Jacobian Vol ; }
  { Region All; Jacobian Sur ; }
    }
  }
  { Name JMatAxi ;
    Case {
  { Region All; Jacobian VolAxi;}
    }
  }
}


Integration {
  { Name GaussIntegration ;
    Case {
      { Type Gauss ;
        Case {
            { GeoElement Triangle    ; NumberOfPoints  7 ; }
{ GeoElement Quadrangle  ; NumberOfPoints  7 ; }
{ GeoElement Tetrahedron ; NumberOfPoints  7 ; }
{ GeoElement Hexahedron  ; NumberOfPoints  7 ; }
{ GeoElement Line        ; NumberOfPoints  7 ; }
        }
      }
    }
  }
}


Formulation {

  { Name Eddy_Formulation_Linear; Type FemEquation ;
    Quantity {
      { Name H; Type Local; NameOfSpace FunctSpA; }
    }
    Equation {
 Galerkin { DtDof[ mu_lin * Dof{H} , {H}]     ; In Stack; Jacobian JMat; Integration GaussIntegration;}
 Galerkin { [ 1/sig[] * Dof{Curl H} , {Curl H}]; In Stack; Jacobian JMat; Integration GaussIntegration;}
    }
  }

  { Name Eddy_Formulation_Nonlinear; Type FemEquation ;
    Quantity {
      { Name H;    Type Local; NameOfSpace FunctSpA; }
  { Name Hpast; Type Local; NameOfSpace FunctSpB; }
    }
    Equation {
 Galerkin { [ 1/sig[]* Dof{Curl H}                , {Curl H}];
  In Stack   ; Jacobian JMat; Integration GaussIntegration;}

 Galerkin { [ 1.0/$DTime * B[{H}]                , {H}];
```

```
 In Iron    ; Jacobian JMat; Integration GaussIntegration;}

 Galerkin { [-1.0/$DTime * B[{Hpast}]             , {H}];
 In Iron    ; Jacobian JMat; Integration GaussIntegration;}

     Galerkin { JacNL [1.0/$DTime * dBdH[{H}] * Dof{H}, {H}];
     In Iron    ; Jacobian JMat; Integration GaussIntegration;}

 Galerkin { [ 1.0/$DTime * mu_lin * Dof{H}   , {H}];
 In CSurface; Jacobian JMat; Integration GaussIntegration;}

 Galerkin { [-1.0/$DTime * mu_lin * {Hpast}       , {H}];
 In CSurface; Jacobian JMat; Integration GaussIntegration;}
    }
  }

  { Name StoreH; Type FemEquation ;
    Quantity {
      { Name H    ; Type Local; NameOfSpace FunctSpA; }
  { Name Hpast; Type Local; NameOfSpace FunctSpB; }
    }
    Equation {
 Galerkin { [ Dof{Hpast}, {Hpast}];
 In Stack; Jacobian JMat; Integration GaussIntegration ; }

 Galerkin { [ -{H}      , {Hpast}];
 In Stack; Jacobian JMat; Integration GaussIntegration ; }
    }
  }
}

Resolution {

  { Name Harmonic_Solution ;
    System {
      { Name T ; NameOfFormulation Eddy_Formulation_Linear ;
        Type ComplexValue; Frequency Freq; }
    }
    Operation {
      Generate[T]; Solve[T]; SaveSolution[T] ;
    }
  }

  { Name Solution_Linear;
    System {
      { Name T; NameOfFormulation Eddy_Formulation_Linear;}
    }
    Operation {
  InitSolution[T];
  TimeLoopTheta[T_Time0,T_TimeMax,T_DTime[], T_Theta[]]{
         Generate[T];
 Solve[T] ;
         SaveSolution[T];
     }
   }
 }

 { Name Solution_Nonlinear;
    System {
      { Name H;    NameOfFormulation Eddy_Formulation_Nonlinear;}
  { Name Hpast; NameOfFormulation StoreH;}
    }
    Operation {
  InitSolution[H];
  InitSolution[Hpast];
  TimeLoopTheta[T_Time0,T_TimeMax,T_DTime[], T_Theta[]]{
    Generate[Hpast]; Solve[Hpast];
    IterativeLoop[maxit, eps, relax] {
```

```
  GenerateJac[H] ; SolveJac[H] ;
}
    SaveSolution[H];
      }
}
 }
}

PostProcessing {

{ Name Harmonic_Solution; NameOfFormulation Eddy_Formulation_Linear;
    Quantity {
{ Name Current_Density_Harmonic; Value { Local{ [{ Curl H }];
 In Stack ; Jacobian JMat ;} } }

{ Name Flux_Density_Harmonic   ; Value { Local{ [ CompZ[mu_lin * {H}]];
 In Stack ; Jacobian JMat ;} } }

{ Name Field_Strength_Harmonic ; Value { Local{ [  CompZ[{H}]];
 In Stack ; Jacobian JMat ;} } }

        { Name Ploss_Linear            ; Value { Integral{ [(((2*Pi*(SquNorm[{Curl H}])/(sig[])))];
         In Stack ; Jacobian JMatAxi; Integration GaussIntegration ;} } }
}
  }
  { Name Solution_Linear; NameOfFormulation Eddy_Formulation_Linear;
    Quantity {
{ Name Current_Density_Linear ; Value { Local{ [{ Curl H }];
 In Stack ; Jacobian JMat ;} } }

{ Name Flux_Density_Linear    ; Value { Local{ [ CompZ[mu_lin * {H}]];
 In Stack ; Jacobian JMat ;} } }

{ Name Field_Strength_Linear  ; Value { Local{ [ CompZ[{H}]];
 In Stack ; Jacobian JMat ;} } }

        { Name Ploss_Linear           ; Value { Integral{ [(((2*Pi*(SquNorm[{Curl H}])/(sig[])))];
         In Stack ; Jacobian JMatAxi; Integration GaussIntegration ;} } }
}
  }
  { Name Solution_Nonlinear; NameOfFormulation Eddy_Formulation_Nonlinear;
    Quantity {
        { Name Current_Density_Nonlinear ; Value { Local{ [{Curl H}]
        ; In Stack ; Jacobian JMat   ;} } }

{ Name Flux_Density_Nonlinear    ; Value { Local{ [ CompZ[mu_non[{H}] * {H}]];
 In Stack ; Jacobian JMat   ;} } }

{ Name Field_Strength_Nonlinear  ; Value { Local{ [ CompZ[{H}]];
In Stack ; Jacobian JMat   ;} } }

        { Name Ploss_Nonlinear           ; Value { Integral{ [(((2*Pi*(SquNorm[{Curl H}])/(sig[])))];
         In Stack ; Jacobian JMatAxi; Integration GaussIntegration ;} } }
  }
 }
}

PostOperation {

{ Name Harmonic_Solution; NameOfPostProcessing Harmonic_Solution;
    Operation {
      Print [Current_Density_Harmonic  ,OnElementsOf Stack  , File "Current_Density_Harmonic.pos"] ;
  Print [Flux_Density_Harmonic     ,OnElementsOf Stack  , File "Flux_Density_Harmonic.pos"] ;
  Print [Field_Strength_Harmonic   ,OnElementsOf Stack  , File "Field_Strength_Harmonic.pos"];
  Print [Field_Strength_Harmonic   ,OnElementsOf Stack  , Format NodeTable, File "Imag_Real_Field.txt"];
  Print [Ploss_Linear[Stack]       ,OnGlobal            , Format Table, File >> "Ploss_Linear.txt"];
}
  }
```

```
  { Name Solution_Linear; NameOfPostProcessing Solution_Linear;
    Operation {
      Print [Current_Density_Linear   ,OnElementsOf Stack, File "Current_Density_Linear.pos"] ;
  Print [Flux_Density_Linear      ,OnElementsOf Stack, File "Flux_Density_Linear.pos"] ;
  Print [Field_Strength_Linear    ,OnElementsOf Stack, File "Field_Strength_Linear.pos"] ;
  Print [Ploss_Linear[Stack]      ,OnGlobal          , Format Table, File >> "Ploss_Linear.txt"];
}
  }
 { Name Solution_Nonlinear; NameOfPostProcessing Solution_Nonlinear;
    Operation {
      Print [Current_Density_Nonlinear,OnElementsOf Stack, File "J_B_NR_N.pos"] ;
  Print [Flux_Density_Nonlinear   ,OnElementsOf Stack, File "B_B_NR_N.pos"] ;
  Print [Field_Strength_Nonlinear ,OnElementsOf Stack, File "H_B_NR_N.pos"] ;
  Print [Ploss_Nonlinear[Stack]   ,OnGlobal          , Format Table, File >> "Ploss_Nonlinear.txt"];
}
  }
}
```

C Gmsh Script: Geometry

```
IronDiv = 15;
RustDiv = 15;
VertDiv = 50;
r = 14e-2;

Point(1) = {0.000e+000+r, 0.000e+000, 0.0, 1.0};
Point(2) = {0.000e+000+r, 6.000e-006, 0.0, 1.0};
Point(3) = {0.000e+000+r, 9.940e-004, 0.0, 1.0};
Point(4) = {0.000e+000+r, 1.006e-003, 0.0, 1.0};
Point(5) = {0.000e+000+r, 1.994e-003, 0.0, 1.0};
Point(6) = {0.000e+000+r, 2.006e-003, 0.0, 1.0};
Point(7) = {0.000e+000+r, 2.994e-003, 0.0, 1.0};
Point(8) = {0.000e+000+r, 3.006e-003, 0.0, 1.0};
Point(9) = {0.000e+000+r, 3.994e-003, 0.0, 1.0};
Point(10) = {0.000e+000+r, 4.006e-003, 0.0, 1.0};
Point(11) = {0.000e+000+r, 4.994e-003, 0.0, 1.0};
Point(12) = {0.000e+000+r, 5.006e-003, 0.0, 1.0};
Point(13) = {0.000e+000+r, 5.994e-003, 0.0, 1.0};
Point(14) = {0.000e+000+r, 6.006e-003, 0.0, 1.0};
Point(15) = {0.000e+000+r, 6.994e-003, 0.0, 1.0};
Point(16) = {0.000e+000+r, 7.006e-003, 0.0, 1.0};
Point(17) = {0.000e+000+r, 7.994e-003, 0.0, 1.0};
Point(18) = {0.000e+000+r, 8.006e-003, 0.0, 1.0};
Point(19) = {0.000e+000+r, 8.994e-003, 0.0, 1.0};
Point(20) = {0.000e+000+r, 9.006e-003, 0.0, 1.0};
Point(21) = {0.000e+000+r, 9.994e-003, 0.0, 1.0};
Point(22) = {0.000e+000+r, 1.001e-002, 0.0, 1.0};
Point(23) = {0.000e+000+r, 1.099e-002, 0.0, 1.0};
Point(24) = {0.000e+000+r, 1.101e-002, 0.0, 1.0};
Point(25) = {0.000e+000+r, 1.199e-002, 0.0, 1.0};
Point(26) = {0.000e+000+r, 1.201e-002, 0.0, 1.0};
Point(27) = {0.000e+000+r, 1.299e-002, 0.0, 1.0};
Point(28) = {0.000e+000+r, 1.301e-002, 0.0, 1.0};
Point(29) = {0.000e+000+r, 1.399e-002, 0.0, 1.0};
Point(30) = {0.000e+000+r, 1.401e-002, 0.0, 1.0};
Point(31) = {0.000e+000+r, 1.499e-002, 0.0, 1.0};
Point(32) = {0.000e+000+r, 1.501e-002, 0.0, 1.0};
Point(33) = {0.000e+000+r, 1.599e-002, 0.0, 1.0};
Point(34) = {0.000e+000+r, 1.601e-002, 0.0, 1.0};
Point(35) = {0.000e+000+r, 1.699e-002, 0.0, 1.0};
Point(36) = {0.000e+000+r, 1.701e-002, 0.0, 1.0};
Point(37) = {0.000e+000+r, 1.799e-002, 0.0, 1.0};
Point(38) = {0.000e+000+r, 1.801e-002, 0.0, 1.0};
Point(39) = {0.000e+000+r, 1.899e-002, 0.0, 1.0};
Point(40) = {0.000e+000+r, 1.901e-002, 0.0, 1.0};
Point(41) = {0.000e+000+r, 1.999e-002, 0.0, 1.0};
Point(42) = {0.000e+000+r, 2.000e-002, 0.0, 1.0};
Point(43) = {2.000e-002+r, 2.000e-002, 0.0, 1.0};
Point(44) = {2.000e-002+r, 1.999e-002, 0.0, 1.0};
Point(45) = {2.000e-002+r, 1.901e-002, 0.0, 1.0};
Point(46) = {2.000e-002+r, 1.899e-002, 0.0, 1.0};
Point(47) = {2.000e-002+r, 1.801e-002, 0.0, 1.0};
Point(48) = {2.000e-002+r, 1.799e-002, 0.0, 1.0};
Point(49) = {2.000e-002+r, 1.701e-002, 0.0, 1.0};
Point(50) = {2.000e-002+r, 1.699e-002, 0.0, 1.0};
Point(51) = {2.000e-002+r, 1.601e-002, 0.0, 1.0};
Point(52) = {2.000e-002+r, 1.599e-002, 0.0, 1.0};
Point(53) = {2.000e-002+r, 1.501e-002, 0.0, 1.0};
Point(54) = {2.000e-002+r, 1.499e-002, 0.0, 1.0};
Point(55) = {2.000e-002+r, 1.401e-002, 0.0, 1.0};
Point(56) = {2.000e-002+r, 1.399e-002, 0.0, 1.0};
Point(57) = {2.000e-002+r, 1.301e-002, 0.0, 1.0};
Point(58) = {2.000e-002+r, 1.299e-002, 0.0, 1.0};
```

```
Point(59) = {2.000e-002+r, 1.201e-002, 0.0, 1.0};
Point(60) = {2.000e-002+r, 1.199e-002, 0.0, 1.0};
Point(61) = {2.000e-002+r, 1.101e-002, 0.0, 1.0};
Point(62) = {2.000e-002+r, 1.099e-002, 0.0, 1.0};
Point(63) = {2.000e-002+r, 1.001e-002, 0.0, 1.0};
Point(64) = {2.000e-002+r, 9.994e-003, 0.0, 1.0};
Point(65) = {2.000e-002+r, 9.006e-003, 0.0, 1.0};
Point(66) = {2.000e-002+r, 8.994e-003, 0.0, 1.0};
Point(67) = {2.000e-002+r, 8.006e-003, 0.0, 1.0};
Point(68) = {2.000e-002+r, 7.994e-003, 0.0, 1.0};
Point(69) = {2.000e-002+r, 7.006e-003, 0.0, 1.0};
Point(70) = {2.000e-002+r, 6.994e-003, 0.0, 1.0};
Point(71) = {2.000e-002+r, 6.006e-003, 0.0, 1.0};
Point(72) = {2.000e-002+r, 5.994e-003, 0.0, 1.0};
Point(73) = {2.000e-002+r, 5.006e-003, 0.0, 1.0};
Point(74) = {2.000e-002+r, 4.994e-003, 0.0, 1.0};
Point(75) = {2.000e-002+r, 4.006e-003, 0.0, 1.0};
Point(76) = {2.000e-002+r, 3.994e-003, 0.0, 1.0};
Point(77) = {2.000e-002+r, 3.006e-003, 0.0, 1.0};
Point(78) = {2.000e-002+r, 2.994e-003, 0.0, 1.0};
Point(79) = {2.000e-002+r, 2.006e-003, 0.0, 1.0};
Point(80) = {2.000e-002+r, 1.994e-003, 0.0, 1.0};
Point(81) = {2.000e-002+r, 1.006e-003, 0.0, 1.0};
Point(82) = {2.000e-002+r, 9.940e-004, 0.0, 1.0};
Point(83) = {2.000e-002+r, 6.000e-006, 0.0, 1.0};
Point(84) = {2.000e-002+r, 0.000e+000, 0.0, 1.0};
Line(1) = {2, 1};
Line(2) = {3, 2};
Line(3) = {4, 3};
Line(4) = {5, 4};
Line(5) = {6, 5};
Line(6) = {7, 6};
Line(7) = {8, 7};
Line(8) = {9, 8};
Line(9) = {10, 9};
Line(10) = {11, 10};
Line(11) = {12, 11};
Line(12) = {13, 12};
Line(13) = {14, 13};
Line(14) = {15, 14};
Line(15) = {16, 15};
Line(16) = {17, 16};
Line(17) = {18, 17};
Line(18) = {19, 18};
Line(19) = {20, 19};
Line(20) = {21, 20};
Line(21) = {22, 21};
Line(22) = {23, 22};
Line(23) = {24, 23};
Line(24) = {25, 24};
Line(25) = {26, 25};
Line(26) = {27, 26};
Line(27) = {28, 27};
Line(28) = {29, 28};
Line(29) = {30, 29};
Line(30) = {31, 30};
Line(31) = {32, 31};
Line(32) = {33, 32};
Line(33) = {34, 33};
Line(34) = {35, 34};
Line(35) = {36, 35};
Line(36) = {37, 36};
Line(37) = {38, 37};
Line(38) = {39, 38};
Line(39) = {40, 39};
Line(40) = {41, 40};
Line(41) = {42, 41};
Line(42) = {43, 42};
```

```
Line(43) = {44, 43};
Line(44) = {45, 44};
Line(45) = {46, 45};
Line(46) = {47, 46};
Line(47) = {48, 47};
Line(48) = {49, 48};
Line(49) = {50, 49};
Line(50) = {51, 50};
Line(51) = {52, 51};
Line(52) = {53, 52};
Line(53) = {54, 53};
Line(54) = {55, 54};
Line(55) = {56, 55};
Line(56) = {57, 56};
Line(57) = {58, 57};
Line(58) = {59, 58};
Line(59) = {60, 59};
Line(60) = {61, 60};
Line(61) = {62, 61};
Line(62) = {63, 62};
Line(63) = {64, 63};
Line(64) = {65, 64};
Line(65) = {66, 65};
Line(66) = {67, 66};
Line(67) = {68, 67};
Line(68) = {69, 68};
Line(69) = {70, 69};
Line(70) = {71, 70};
Line(71) = {72, 71};
Line(72) = {73, 72};
Line(73) = {74, 73};
Line(74) = {75, 74};
Line(75) = {76, 75};
Line(76) = {77, 76};
Line(77) = {78, 77};
Line(78) = {79, 78};
Line(79) = {80, 79};
Line(80) = {81, 80};
Line(81) = {82, 81};
Line(82) = {83, 82};
Line(83) = {84, 83};
Line(84) = {1, 84};
Line(85) = {83, 2};
Line(86) = {82, 3};
Line(87) = {81, 4};
Line(88) = {80, 5};
Line(89) = {79, 6};
Line(90) = {78, 7};
Line(91) = {77, 8};
Line(92) = {76, 9};
Line(93) = {75, 10};
Line(94) = {74, 11};
Line(95) = {73, 12};
Line(96) = {72, 13};
Line(97) = {71, 14};
Line(98) = {70, 15};
Line(99) = {69, 16};
Line(100) = {68, 17};
Line(101) = {67, 18};
Line(102) = {66, 19};
Line(103) = {65, 20};
Line(104) = {64, 21};
Line(105) = {63, 22};
Line(106) = {62, 23};
Line(107) = {61, 24};
Line(108) = {60, 25};
Line(109) = {59, 26};
Line(110) = {58, 27};
```

```
Line(111) = {57, 28};
Line(112) = {56, 29};
Line(113) = {55, 30};
Line(114) = {54, 31};
Line(115) = {53, 32};
Line(116) = {52, 33};
Line(117) = {51, 34};
Line(118) = {50, 35};
Line(119) = {49, 36};
Line(120) = {48, 37};
Line(121) = {47, 38};
Line(122) = {46, 39};
Line(123) = {45, 40};
Line(124) = {44, 41};
Line Loop(125) = {1, 85, 83, 84};
Plane Surface(126) = {125};
Line Loop(127) = {2, 86, 82, -85};
Plane Surface(128) = {127};
Line Loop(129) = {3, 87, 81, -86};
Plane Surface(130) = {129};
Line Loop(131) = {4, 88, 80, -87};
Plane Surface(132) = {131};
Line Loop(133) = {5, 89, 79, -88};
Plane Surface(134) = {133};
Line Loop(135) = {6, 90, 78, -89};
Plane Surface(136) = {135};
Line Loop(137) = {7, 91, 77, -90};
Plane Surface(138) = {137};
Line Loop(139) = {8, 92, 76, -91};
Plane Surface(140) = {139};
Line Loop(141) = {9, 93, 75, -92};
Plane Surface(142) = {141};
Line Loop(143) = {10, 94, 74, -93};
Plane Surface(144) = {143};
Line Loop(145) = {11, 95, 73, -94};
Plane Surface(146) = {145};
Line Loop(147) = {12, 96, 72, -95};
Plane Surface(148) = {147};
Line Loop(149) = {13, 97, 71, -96};
Plane Surface(150) = {149};
Line Loop(151) = {14, 98, 70, -97};
Plane Surface(152) = {151};
Line Loop(153) = {15, 99, 69, -98};
Plane Surface(154) = {153};
Line Loop(155) = {16, 100, 68, -99};
Plane Surface(156) = {155};
Line Loop(157) = {17, 101, 67, -100};
Plane Surface(158) = {157};
Line Loop(159) = {18, 102, 66, -101};
Plane Surface(160) = {159};
Line Loop(161) = {19, 103, 65, -102};
Plane Surface(162) = {161};
Line Loop(163) = {20, 104, 64, -103};
Plane Surface(164) = {163};
Line Loop(165) = {21, 105, 63, -104};
Plane Surface(166) = {165};
Line Loop(167) = {22, 106, 62, -105};
Plane Surface(168) = {167};
Line Loop(169) = {23, 107, 61, -106};
Plane Surface(170) = {169};
Line Loop(171) = {24, 108, 60, -107};
Plane Surface(172) = {171};
Line Loop(173) = {25, 109, 59, -108};
Plane Surface(174) = {173};
Line Loop(175) = {26, 110, 58, -109};
Plane Surface(176) = {175};
Line Loop(177) = {27, 111, 57, -110};
Plane Surface(178) = {177};
```

```
Line Loop(179) = {28, 112, 56, -111};
Plane Surface(180) = {179};
Line Loop(181) = {29, 113, 55, -112};
Plane Surface(182) = {181};
Line Loop(183) = {30, 114, 54, -113};
Plane Surface(184) = {183};
Line Loop(185) = {31, 115, 53, -114};
Plane Surface(186) = {185};
Line Loop(187) = {32, 116, 52, -115};
Plane Surface(188) = {187};
Line Loop(189) = {33, 117, 51, -116};
Plane Surface(190) = {189};
Line Loop(191) = {34, 118, 50, -117};
Plane Surface(192) = {191};
Line Loop(193) = {35, 119, 49, -118};
Plane Surface(194) = {193};
Line Loop(195) = {36, 120, 48, -119};
Plane Surface(196) = {195};
Line Loop(197) = {37, 121, 47, -120};
Plane Surface(198) = {197};
Line Loop(199) = {38, 122, 46, -121};
Plane Surface(200) = {199};
Line Loop(201) = {39, 123, 45, -122};
Plane Surface(202) = {201};
Line Loop(203) = {40, 124, 44, -123};
Plane Surface(204) = {203};
Line Loop(205) = {41, 42, 43, -124};
Plane Surface(206) = {205};
Physical Line(207) = {1,2,3,4,5,6,7,8,9,10,11,12,13,14,15,16,17,18,19,20,21,
22,23,24,25,26,27,28,29,30,31,32,33,34,35,36,37,38,39,
40,41,42,43,44,45,46,47,48,49,50,51,52,53,54,55,56,57,
58,59,60,61,62,63,64,65,66,67,68,69,70,71,72,73,74,75,
76,77,78,79,80,81,82,83,84};

IRON_ID= 208;
CSURFACE_ID= 209;

Physical Surface(IRON_ID) = {128,132,136,140,144,148,152,156,160,164,168,172,176,180,
184,188,192,196,200,204};
Physical Surface(CSURFACE_ID) = {126,130,134,138,142,146,150,154,158,162,166,170,174,178,
182,186,190,194,198,202,206};
Transfinite Line{2,4,6,8,10,12,14,16,18,20,22,24,26,28,30,32,34,36,38,
40,82,80,78,76,74,72,70,68,66,64,62,60,58,56,54,52,50,48,46,44} = IronDiv Using Bump 0.05;
Transfinite Line{1,3,5,7,9,11,13,15,17,19,21,23,25,27,29,31,33,35,37,
39,41,83,81,79,77,75,73,71,69,67,65,63,61,59,57,55,53,51,49,47,45,43} = RustDiv;
Transfinite Line{-84,85,86,87,88,89,90,91,92,93,94,95,96,97,98,99,100,
101,102,103,104,105,106,107,108,109,110,111,112,113,114,115,
116,117,118,119,120,121,122,123,124,42} = VertDiv Using Bump 0.05;
Transfinite Surface{126} ={1, 2, 83, 84};
Transfinite Surface{128} ={2, 3, 82, 83};
Transfinite Surface{130} ={3, 4, 81, 82};
Transfinite Surface{132} ={4, 5, 80, 81};
Transfinite Surface{134} ={5, 6, 79, 80};
Transfinite Surface{136} ={6, 7, 78, 79};
Transfinite Surface{138} ={7, 8, 77, 78};
Transfinite Surface{140} ={8, 9, 76, 77};
Transfinite Surface{142} ={9, 10, 75, 76};
Transfinite Surface{144} ={10, 11, 74, 75};
Transfinite Surface{146} ={11, 12, 73, 74};
Transfinite Surface{148} ={12, 13, 72, 73};
Transfinite Surface{150} ={13, 14, 71, 72};
Transfinite Surface{152} ={14, 15, 70, 71};
Transfinite Surface{154} ={15, 16, 69, 70};
Transfinite Surface{156} ={16, 17, 68, 69};
Transfinite Surface{158} ={17, 18, 67, 68};
Transfinite Surface{160} ={18, 19, 66, 67};
Transfinite Surface{162} ={19, 20, 65, 66};
Transfinite Surface{164} ={20, 21, 64, 65};
```

```
Transfinite Surface{166} ={21, 22, 63, 64};
Transfinite Surface{168} ={22, 23, 62, 63};
Transfinite Surface{170} ={23, 24, 61, 62};
Transfinite Surface{172} ={24, 25, 60, 61};
Transfinite Surface{174} ={25, 26, 59, 60};
Transfinite Surface{176} ={26, 27, 58, 59};
Transfinite Surface{178} ={27, 28, 57, 58};
Transfinite Surface{180} ={28, 29, 56, 57};
Transfinite Surface{182} ={29, 30, 55, 56};
Transfinite Surface{184} ={30, 31, 54, 55};
Transfinite Surface{186} ={31, 32, 53, 54};
Transfinite Surface{188} ={32, 33, 52, 53};
Transfinite Surface{190} ={33, 34, 51, 52};
Transfinite Surface{192} ={34, 35, 50, 51};
Transfinite Surface{194} ={35, 36, 49, 50};
Transfinite Surface{196} ={36, 37, 48, 49};
Transfinite Surface{198} ={37, 38, 47, 48};
Transfinite Surface{200} ={38, 39, 46, 47};
Transfinite Surface{202} ={39, 40, 45, 46};
Transfinite Surface{204} ={40, 41, 44, 45};
Transfinite Surface{206} ={-41, 42, 43, 44};

Recombine Surface{126,128,130,132,134,136,138,140,142,144,
146,148,150,152,154,156,158,160,162,164,166,168,170,172,174,
176,178,180,182,184,186,188,190,192,194,196,198,200,202,204,
206};
```